2018•2019

Faculteit Industriële ingenieurswetenschappen

master in de industriële wetenschappen: nucleaire technologie

Masterthesis

Materials research for nuclear fusion energy: analysing the flow properties of eurofer97

PROMOTOR :

Prof. dr. Wouter SCHROEYERS

PROMOTOR :

Dhr. Giovanni BONNY

COPROMOTOR :

Dhr. Dmitry TERENTYEV

Alexander Vermeersch

Scriptie ingediend tot het behalen van de graad van master in de industriële wetenschappen: nucleaire technologie, afstudeerrichting nucleaire technieken / medisch nucleaire technieken

Gezamenlijke opleiding UHasselt en KU Leuven

UHASSELT

KU LEUVEN

UHASSELT

KU LEUVEN

2018•2019

Faculteit Industriële ingenieurswetenschappen

master in de industriële wetenschappen: nucleaire technologie

Masterthesis

Materials research for nuclear fusion energy: analysing the flow properties of eurofer97

PROMOTOR :

Prof. dr. Wouter SCHROEYERS

PROMOTOR :

Dhr. Giovanni BONNY

COPROMOTOR :

Dhr. Dmitry TERENTYEV

Alexander Vermeersch

Scriptie ingediend tot het behalen van de graad van master in de industriële wetenschappen: nucleaire technologie, afstudeerrichting nucleaire technieken / medisch nucleaire technieken

UHASSELT KU LEUVEN

WORDS OF GRATITUDE

This master's thesis is the report surrounding the research I have conducted during my final year of study as a student in Master of Nuclear Engineering Technology, an education at the University of Hasselt and the Catholic University of Leuven. This work was performed in association with SCK●CEN and would not have been possible without the resources and support they provided.

Firstly, I would like to express my deepest gratitude towards Dr. Ir. Dmitry Terentyev and Dr. Ir. Giovanni Bonny, who guided me through the learning and writing process of this master's thesis. Their assistance in seeing this work through to completion was invaluable.

Secondly, I thank Prof. dr. Wouter Schroeyers for aiding me in improving this work by reviewing my findings. I also thank the staff of the lab at SCK●CEN where I performed my tests for teaching me how to use their equipment and helping me when it was necessary.

Working on this master's thesis with these people has been a tremendous learning experience and a privilege.

Alexander Vermeersch

TABLE OF CONTENTS

LIST OF TABLES

LIST OF FIGURES

ABSTRACT

In dit werk werden verscheidene mechanische eigenschappen van een ferritisch/martensitisch staal met verlaagde activatie (RAFM) geanalyseerd en vergeleken met het Europese referentiemateriaal, Eurofer97. Dit onderzochte RAFM-staal heeft een specifieke warmtebehandeling ondergaan met de bedoeling zijn mechanische eigenschappen te optimaliseren en is bedoeld om als structureel materiaal gebruikt te worden in fusiereactoren. De mechanische eigenschappen en het breukoppervlak werden op volgende manieren geanalyseerd: de Vickers-hardheidsmeter, de kerfslagproef, de trekproef en microscopie. In deze thesis zijn de eigenschappen die centraal staan de hardheid van het materiaal, de ductiel naar brosse breuk transitie temperatuur (DBTT) en zijn vloeigrens op zowel kamertemperatuur als op hoge temperatuur.
Na de analyse van de mechanische eigenschappen werd een nieuwe, experimentele manier voor het benaderen van het materiaal zijn vloeigrens op verschillende temperaturen onderzocht. Het doel is om de volledige temperatuurafhankelijkheid van de vloeigrens uit een enkel proefstuk af te leiden. Indien deze techniek succesvol is, zal deze zorgen voor een grote reductie in het aantal proefstukken van een materiaal die nodig zijn voor het bepalen van deze afhankelijkheid. Indien het gaat om het testen van bestraalde monsters kan dit de kosten significant verlagen.

ABSTRACT

In this work, the flow properties of a lab-cast reduced activation ferritic/martensitic (RAFM) steel were analysed and compared to the reference European RAFM material, Eurofer97. This steel has passed dedicated heat treatment in order to optimize its mechanical properties and is intended for use as a structural material in nuclear fusion reactors. Its flow properties and fracture surface were examined through the execution of the following tests: Vickers hardness test, Charpy impact test, tensile test and microscopy. In this thesis, the central properties that are to be examined are the material's hardness, the ductile-to-brittle transition temperature (DBTT) and its yield strength at both room temperature and elevated temperature.

Following the assessment of the flow properties, a new experimental technique was explored for estimating the 0.2% yield strength of a material at different temperatures. The objective is to assess the temperature dependent 0.2% yield strength from a single sample. If proven successful, this technique will greatly reduce the number of samples needed to investigate the ductility range. In the context of testing irradiated samples, this could significantly reduce costs.

1 INTRODUCTION

1.1 Nuclear fusion reactors

The Tokamak, developed in the late 1960s, is a magnetic fusion device where hydrogen fuel is present in the form of a hot, charged plasma [1]. Magnets are used to prevent the plasma from touching the vessel walls. The goal is to induce nuclear reactions between the deuterium (D) and tritium (T) nuclei, creating helium (He) and a fast neutron (n) with a large amount of energy.

$$D + T \rightarrow {}^{4}He\ (3.56\ MeV) + n\ (14.03\ MeV) \qquad (1)$$

These neutrons escape from the plasma and make it to the breeding blanket, where they react with lithium atoms, creating helium, tritium and new fast neutrons (Fig. 1).

$$n + {}^{6}Li \rightarrow {}^{4}He\ T + n\ (4.68\ MeV) \qquad (2)$$

The neutrons created in this process can collide again with lithium and helium isotopes resulting in the production of even more tritium, which is re-injected into the plasma and used as fuel. The significance of this cycle is that tritium nuclei have a short lifetime and must therefore be created while the reactions are going on. Besides Li, the breeding blanket contains a neutron multiplier, usually Pb or Be.
The fusion reaction and the tritium production are exothermic, meaning that much like a conventional power plant, the heat created is used to produce steam and electricity through turbines and generators.

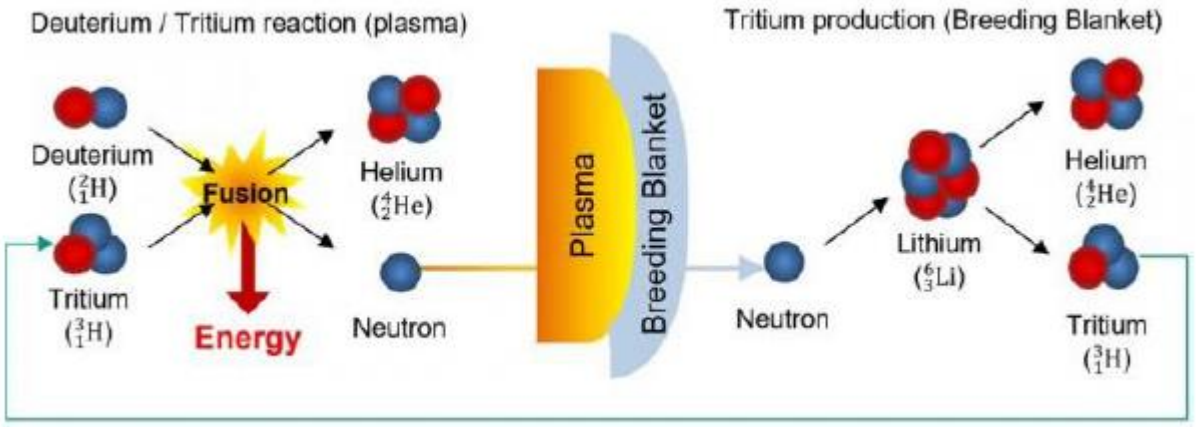

Figure 1: Tritium breeding inside a fusion reactor [2].

1.2 Irradiation damage

During nuclear fusion, energetic, neutrons will irradiate the structural materials of the reactor. This causes displacements in atoms, resulting in lattice defects. The resulting damage is measured in displacements per atom (dpa). Irradiation damage delivered to a material affects the microstructure and hence, mechanical properties. The materials inside fusion reactors will receive much higher neutron doses than current generation fission reactors. On top of that, in order to maintain high efficiency in fusion reactors, the operational temperature is far greater (450-650°C or higher, depending on the design) than the temperature found in fission reactors, which is around 300°C. This causes extra strain on the material of the reactor.

In the high temperature conditions of fusion reactors, the following materials are of interest: ferritic/martensitic (F/M) steels, vanadium (V) alloys, oxide dispersion strengthened (ODS) F/M steels and SiC composites (still under development). Figure 2 shows the dpa and temperature that structural elements of various reactor concepts will need to be able to withstand [3].

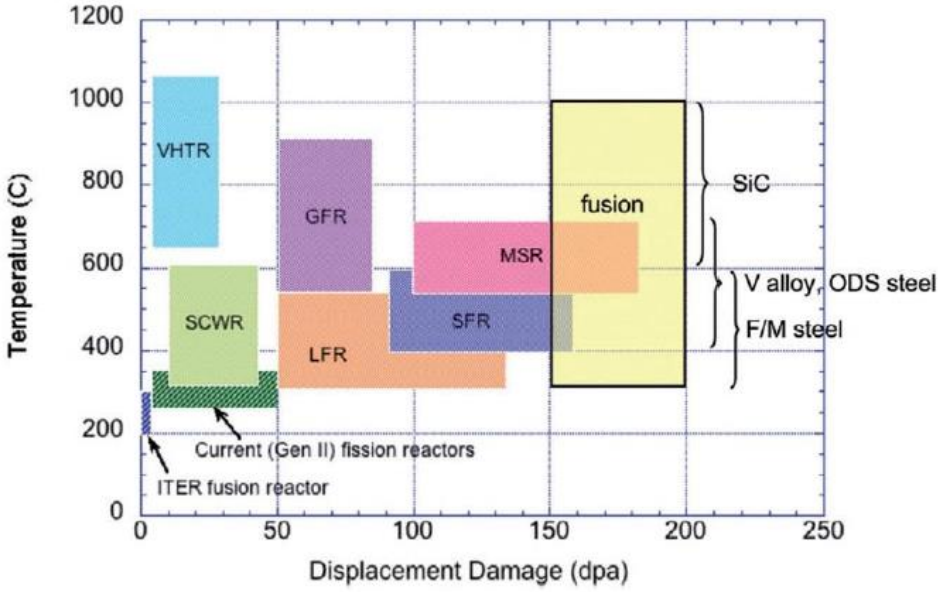

Figure 2: Service temperatures and displacement damage for structural materials in several nuclear setups [3]. Generation IV fission reactors: VHTR – very high temperature reactor; SCWR – super critical water reactor; GFR gas cooled fast reactor; LFR – lead cooled fast reactor; SFR – sodium cooled fast reactor; MSR – molten salt reactor.

At temperatures below 40% of the melting temperature and starting at neutron doses of approximately 0.1 dpa, hardening and embrittlement of the material is induced by irradiation [3]. This causes the ductile-to-brittle transition temperature (DBTT) to increase and a reduction of the upper shelf energy (USE) (Fig. 3) [4]. Structural materials inside a reactor are not allowed to behave in a brittle way, hence, the DBTT of materials used in a reactor must stay sufficiently below the operational temperature of the reactor.

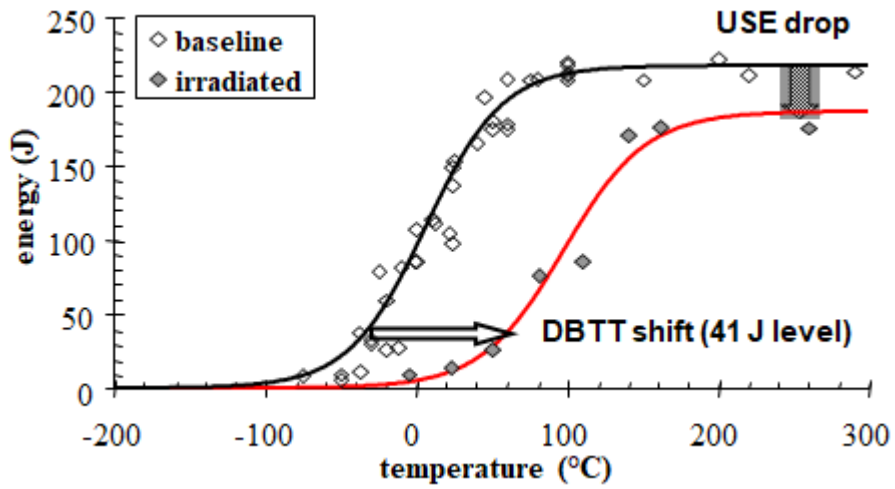

Figure 3: DBTT shift and USE drop due to irradiation embrittlement [5].

Between 30% and 60% of the melting temperature, the previous forms of hardening and embrittlement decrease. However, the microstructure is vulnerable to change when exposed to neutron doses resulting in an excess of 10 dpa, negatively affecting mechanical properties [4]. A further decrease in functionality of structural components in this temperature range is caused by void swelling and irradiation creep. F/M steels possess good swelling resistance, which is the main reason why F/M steels are commonly used [6]. Another advantage of F/M steels compared to austenitic stainless steels is the limited production of He. Irradiation induces transmutations, creating hydrogen and helium, which are sources of radioactivity and He-embrittlement. Besides specific irradiation effects, conventional thermal creep reduces the lifetime of structural steels due to irreversible deformations.

The effect of irradiation on a material can also be seen in its stress-strain curve. An irradiated material will have a higher yield strength than a non-irradiated one, but will also behave more brittle, which is reflected in the reduction of accumulated strain in the tensile test (Fig. 4). This phenomenon is called irradiation hardening and associated embrittlement.

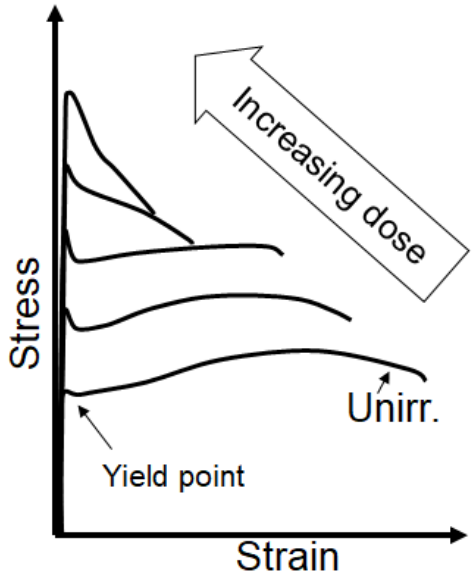

Figure 4: The yield strength increases due to irradiation hardening and the accumulated strain is reduced due to the associated embrittlement.

1.3 Reduced activation F/M steels

In conventional F/M steels, the high accumulated neutron dose in a nuclear fusion reactor would induce long-term radioactivity inside the material, creating harmful waste. For this reason, reduced activation F/M (RAFM) steels were proposed as an alternative. These steels are made by substituting alloying elements like Mo, Nb, Co and Ni with elements that have a lower radiological impact but similar metallurgical effects such as W, V and Ta [7]. RAFM steels that are currently of interest to fusion programs are given in Table 1. Tests on 9Cr1WVTa steel (the names of the elements refer to what elements are present in the steel, the numbers indicate the wt% in which an element is present), also called Eurofer97, revealed it has similar properties to classic 9Cr1Mo steels, meaning good thermal conductivity and low swelling behaviour, even at high doses (150 dpa) and temperature (400°C – 650°C) [8].

Table 1: Chemical composition of RAFM steels currently of interest [4],[9],[10].

Program	[wt%]	C	Mn	Si	Cr	N	W	V	Ta	B
Europe	**EU97**	0.11	0.40	0.03	9	0.030	1	0.25	0.08	0.005
Japan	**F82H**	0.10	0.50	0.2	8	<0.01	2	0.20	0.04	0.003
USA	**ORNL**	0.10	0.40	0.3	9	-	2	0.25	0.07	-
India	**INRAFM**	0.10	0.50	0.03	9	0.025	1.3	0.23	0.08	<0.001
China	**CLAM**	0.10	0.45	0.1	9	0.025	1.5	0.20	0.15	-

The large fraction of Cr present in RAFM steels is responsible for its good resistance against corrosion. Ta (substituting Nb) controls austenitic grain growth, reduces the DBTT shift and improves the alloy's strength. W atoms are larger than Fe, creating a strengthening effect. Carbide and nitride formers like V and Ta improve the resistance to high temperature creep.

RAFM steels are envisaged in breeding blanket modules of the fusion reactor (Fig. 5). The tritium breeding blanket is an essential component to ensure a closed tritium fuel cycle inside the fusion reactor. In ITER, the divertor is made of W and the first wall of Be. In DEMO, W is a candidate for both the divertor and the first wall. Therefore, next to the RAFM steels discussed previously, W is also an element that requires thorough investigation regarding its behaviour in high neutron flux environments.

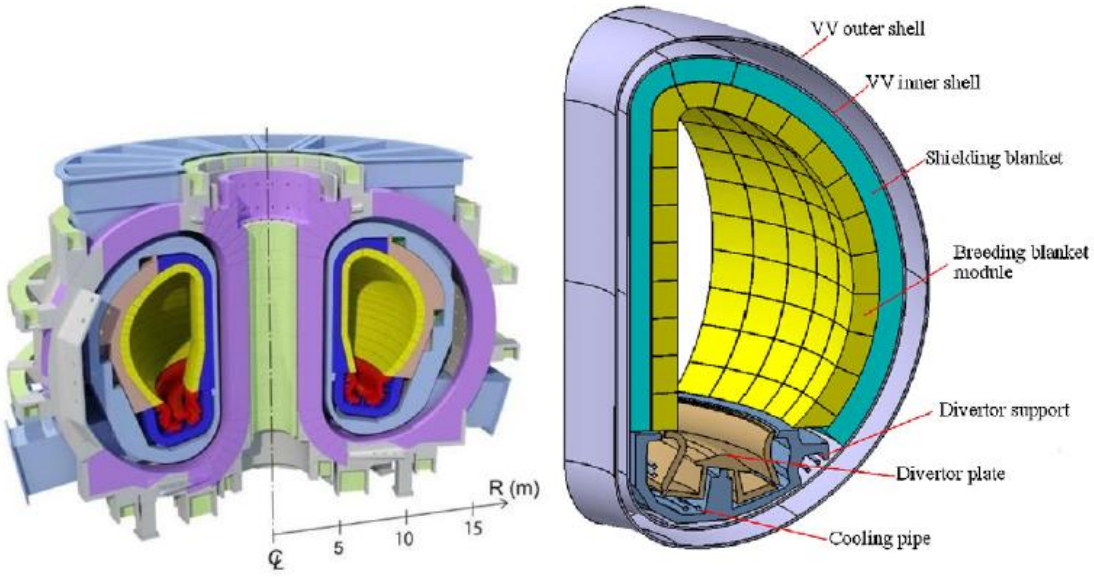

Figure 5: DEMO fusion reactor with breeding blanket modules (yellow) [1].

The efficiency of a fusion reactor depends on the operating temperature. Operating at a higher temperature (650°C) results in an increased efficiency and would therefore be beneficial. However, RAFM steels are subject to significant thermal creep and mechanical degradation at temperatures around 650°C. A material with a temperature exceeding 40% of its melting temperature encounters creep deformation, leading to fractures at loads well below the materials yield stress [11]. This presents a problem since it must be assured that no structural materials may significantly deform or fail under deviations from the service load. When looking at the breeding blanket, the structural materials must be able to withstand a stress of 100 MPa for 10^5 hours at operating temperature without fracture. According to the creep database and assuming an operating temperature of 650°C, EU97 does not meet these requirements [8], [12], [13]. Hence, improvements to the steel are necessary.

1.4 Relation between microstructure and flow properties

The microstructure of RAFM steels is that of a tempered martensitic microstructure with a high dislocation density and high precipitate density (Fig. 6). Exposure to high temperature allows the microstructures to evolve towards a thermodynamic equilibrium. This means a microstructure with less defects and large precipitates in the bulk and grain boundaries. This results in a larger grain size, lower dislocation density and fewer precipitates, which negatively impact the flow properties.

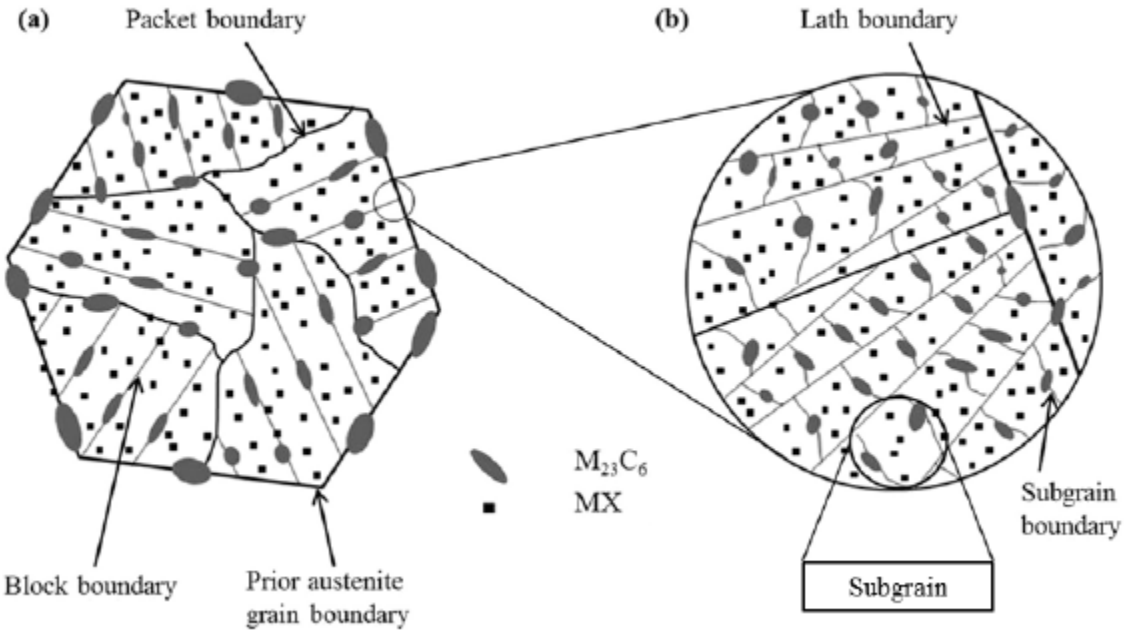

Figure 6: Tempered martensitic structure of Eurofer97 with M23C6 and MX precipitates [14].

The block size affects the strength of the steel according to the following formula:

$$\Delta\sigma_{gb} \approx \frac{BMGb}{\sqrt{d_g}} \qquad (3)$$

This relation shows that a smaller grain size relates to a greater strength. The act of reducing the grain sizes is called grain refinement and is the only strengthening mechanism that does not negatively affect the materials toughness. Adding 0.1 wt% Ta to the composition of a RAFM steel reduces the austenite grain size considerably, due to the formation of small TaC carbides along the austenite grain boundaries. These carbides obstruct the growth of austenitic grains. In turn, upon quenching, the smaller austenitic grains result in a martensite with smaller block size, thereby effectively strengthening the material [15].

In order to create a tempered martensitic microstructure, the steel undergoes a quench and temper (Q&T) treatment (Fig. 7). This Q&T treatment consists of an austenization stage (normalization) followed by a quenching and tempering stage. The austenization temperature is chosen well above the minimal austenization temperature (Ac3). This ensures complete austenite formation.

The final tempering stage influences the precipitate distribution of carbo-nitrides. Its purpose is to pin the grain boundaries and dislocations in place, which improves the material's creep resistance.

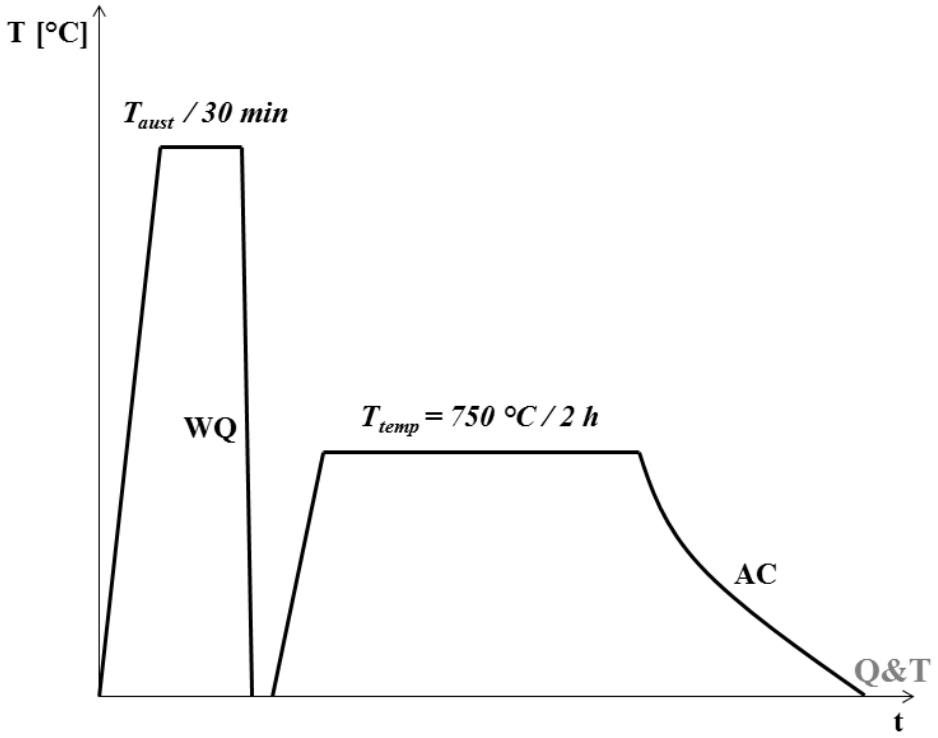

Figure 7: Q&T treatment consisting of an austenization stage (normalization), water quench (WQ), a tempering stage and air cooling (AC).

1.5 Miniaturization

Miniaturized testing brings a significant reduction in both cost and time required for the assessment of new materials using existing test reactors and future irradiation capacities presented by the Myrrha project [16] and IFMIF facility [17].

In normal circumstances, the design and safety analysis require the material's properties to be derived from mechanical tests with well-defined standards, which ensures reproducible results under controlled conditions. In nuclear installations, it is important to consider the effect irradiation has on these properties to ensure structural integrity of components in service. The issue here is that the cost of irradiating a material is high while the irradiation volume is limited, making it very costly to irradiate a standardized specimen. Therefore, it is of great interest to the nuclear industry and material's R&D to transfer the properties obtained from sub-miniaturized specimen to engineering accepted formats [18].

Another way to reduce costs is to reduce the number of samples needed for destructive tests, such as tensile and Charpy tests. On a yield strength vs temperature curve, irradiation hardening causes the curve to shift towards a higher yield strength (Fig. 8). This new stress-strain curve must be mapped with new tests on expensive samples. Moreover, if this shift causes the yield strength to exceed the fracture stress on a temperature where it previously did not, when tested, this could result in a fractured sample that did not reach its yield strength. A measurement like that holds no information of value and therefore wastes an expensive sample. One of the objectives of this work is to examine a new, unconventional way of measuring, which should significantly reduce the number of samples needed to construct the stress-strain curve.

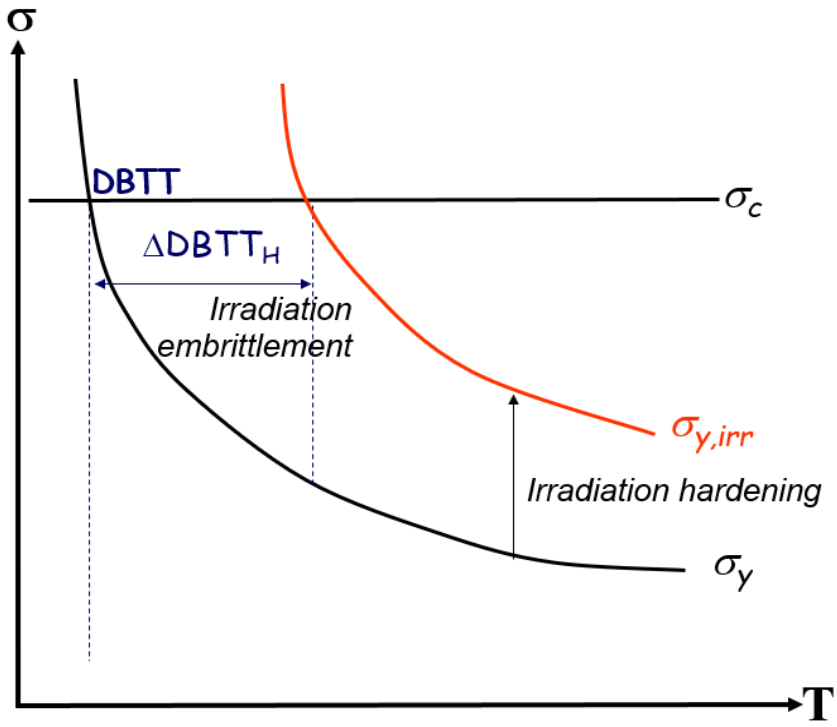

Figure 8: DBTT shift due to irradiation of a material. σ_y denotes the yield strength while σ_c denotes the critical stress for cleavage.

2 OBJECTIVES

In this work, there are two central objectives. The first objective is to analyse the flow properties of lab-cast Eurofer that passed a dedicated heat treatment through the conventional testing methodology and in the process, gain familiarity with executing some of the more common analytical techniques used to characterize materials properties. This includes executing the Vickers hardness test, the Charpy impact test and the tensile test. These results are then compared to the flow properties of regular Eurofer97 in order to determine if the heat treatment yields significant and favourable changes to its properties for application as a structural material in a fusion reactor.

The second objective is to test a new, non-conventional way of deriving the yield strength of a material over a wide range of temperatures without the need to use a different sample at every temperature. If proven successful, this new technique would greatly reduce the number of samples needed for determining the temperature dependence of the yield strength. In the context of testing irradiated samples, this saves reactor space and hence, money.
This objective is divided into three steps. Firstly, validation of the approach. It must be verified that an interrupted tensile test remains representative of a standard tensile test. Secondly, training and execution of the new procedure. Lastly, performing the procedure to derive the temperature dependence of the yield stress and comparing it to other measurements to judge how the results from the new procedure compare to the standard procedure.

3 MATERIALS & METHODS

The flow properties of Eurofer97 are derived from three different types of tests. Firstly, the Vickers hardness test, which measures the hardness of a sample and its ability to resist surface deformations. Secondly, the Charpy test, from which one can deduce if a sample is brittle or ductile and at which temperature transition occurs. Finally, the tensile test, which measures how much stress a sample can take before plastic deformation and fracture occurs.

3.1 Materials

The materials used throughout this work are Chinese low activation martensitic (CLAM) steel, P91, two types of tungsten, regular Eurofer97 and lab-cast Eurofer. In this part, a description will be given of what each material is and why they are of interest.
The nominal chemical composition (wt%) of CLAM steel is: 0.1 ± 0.02 C, 9 ± 0.5 Cr, 1.5 ± 0.2 W, 0.15 ± 0.02 Ta, 0.2 ± 0.02 V, 0.45 ± 0.05 Mn, balance Fe. The heat treatment is a normalization at 980 °C for 30 min and then cooling in air to room temperature and tempering at 760°C for 90 min and then cooling in air to room temperature [19]. CLAM steel has a hardness of 204 HV and can be hardened to 230 HV with specific thermal treatment (1100 hours at 600°C) [20].
This thermal treatment results in a microstructure of tempered martensite with precipitates of carbides, M23C6, and vanadium/niobium rich carbo-nitride of the type MX (M = V or Nb and X = C or N). The presence of carbide precipitates improves the creep rupture strength due to precipitation hardening. CLAM steel is a RAFM steel that is a candidate material for fusion applications as a structural material. The DBTT of CLAM steel is about -52°C.
The chemical composition of P91 is given in table 2. P91 is a commonly used material for the construction of pipes (“P91”) and tubes (“T91”). The hardness of virgin P91 is 225 HV [20]. P91 is commonly used for high temperature applications in the regular industry.

Table 2: Chemical composition of P91 [21].

P91	C	Si	Mn	P	S	AL	Cr	Cu	Mo	N	Nb	Ni	V
Min%	0.08		0.30				8.0		0.85	0,030	0,060		0.18
Max %	0.12	0.50	0.60	0,020	0.005	0,040	9.50	0.30	1.05	0,070	0,100	0.30	0.25

The two types of tungsten in this work are referred to as “AL” and “LL”. The A in AL means that the material is Plansee produced ITER grade tungsten that is double hammered (IGP). The first L in LL means the material is Chinese produced ITER grade tungsten that was rolled (CEFTR). The L as the second initial indicates the samples were cut in the longitudinal direction. Tungsten can be used for construction of the first wall and the divertor of a nuclear fusion reactor.

Eurofer97 is a RAFM steel based on P91 and has similar physical properties. The idea behind Eurofer97 is that it exchanges the elements that tend to become radioactive through neutron absorption in favour of elements with a lower radiological impact such as W, V and Ta. The compositions of Eurofer97 and the lab-casted version used in this work are given in Table 3. The DBTT of standard Eurofer97 is -80°C [22].

Table 3: Chemical composition of Eurofer97 and lab-cast Eurofer [23].

[wt%]	C	Si	Mn	P	S	N	V	Ta	W	Cr	Fe
EU97-2	0.09-0.12	0.05	0.2-0.6	0.005	0.005	0.015-0.045	0.15-0.25	0.10-0.14	1-1.2	8.5-9.5	Bal.
0.09Ta	0.11	0.038	0.40	0.0023	0.0029	0.011	0.22	0.086	1.0	9.3	Bal.

This lab-cast Eurofer (referred to as "M474") originates from a cast weighing approximately 100 kg of which, after removing the head of the ingot, which contains porosities, 55-60 kg of the material remains available. A slice of a few mm thick was cut from the ingot to determine the composition of each cast from the middle of this slice. Each cast was cut into six pieces (120x120x70 mm^3), then reheated to 1250°C for one hour and hot rolled according to the following scheme in Table 4.

Table 4: Hot rolling schedule of lab-cast Eurofer.

Hot rolling schedule.	*Initial*	*Pass 1*	*Pass 2*	*Pass 3*	*Pass 4*	*Pass 5*	*Pass 6*
Reduction (%)	-	19.5	25	30	30	30	30
Temperature (°C)	1200	1200	1150	1100	960	900	850
Final thickness (mm)	70	56	42	30	21	14	10

This material then passed dedicated heat treatment to optimize its mechanical properties (Table 5).

Table 5: Heat treatment schedule of lab-cast Eurofer.

Material	T_{aust} [°C]	t_{aust} [min]	Cooling	T_{temp} [°C]	t_{temp} [min]	Cooling
M474A	880	30	Water quenching	750	120	Air cooling

The purpose of these treatments is to improve the flow properties of this batch of lab-cast Eurofer97 compared to regular Eurofer. The final chemical composition achieved is shown in Table 6 and the minor alloying impurities are shown in Table 7.

Table 6: Chemical composition of lab-cast Eurofer.

Request	C	Mn	Si	Cr	W	N	V	Ta
Target	0.1100	0.4000	0.0370	9.1000	1.0000	0.0110	0.2300	0.086
Max	0.1250	0.4400	0.0550	9.6000	1.2000	0.0200	0.2550	0.126
Min	0.0950	0.3600	0.0250	8.6000	0.8000	0.0060	0.2050	0.046
Realized	0.1120	0.4080	0.029	9.1240	0.9770	0.0123	0.2400	0.085

Table 7: Minor alloying impurities in lab-cast Eurofer.

[wt%]	Mn	Si	P	S	Al	Ti	Nb	Cu	Ni	O	Mo
M474			*0.0062*	*0.0013*	*0.0063*	*0.0014*	*0.0020*	*0.0063*	*0.0050*	*0.0014*	*0.0018*

3.2 Scanning electron microscope

The scanning electron microscope (SEM) performs a type of electron microscopy by scanning the surface of an object with a highly focused electron beam (Fig. 9). The electrons carry large amounts of kinetic energy and interact with the sample, producing various types of signals such as secondary electrons, (diffracted) back-scattered electrons and characteristic X-rays. Secondary electrons produce the SEM image, diffracted backscattered electrons are used to determine crystal structures and grain orientations of the material and X-rays can be used to identify elements [24].
This is a non-destructive analysis method and due to the very narrow electron beam, an SEM has a large depth of field, giving an almost three-dimensional appearance, making it ideal for understanding structures on the surface of the material.

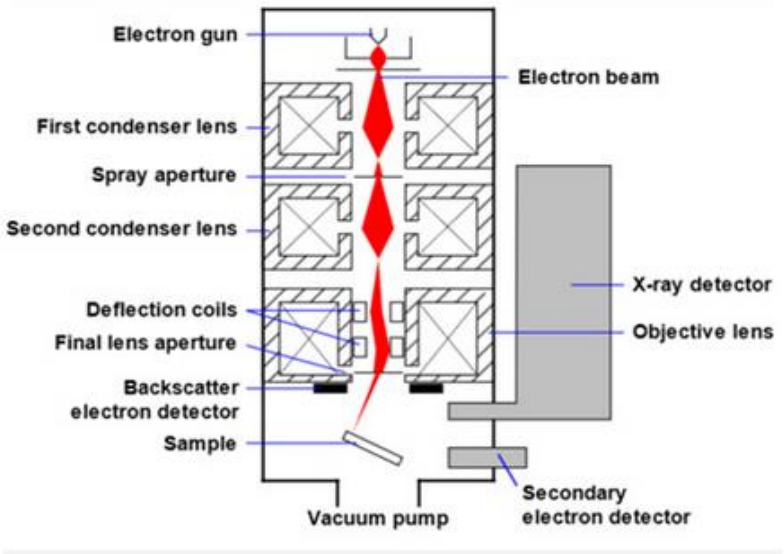

Figure 9: Schematic representation of a scanning electron microscope.

3.3 Charpy impact test

The Charpy impact test determines the amount of energy absorbed by a material during deformation. This test is a tool to study the ductile-brittle transition. In this test, a pendulum of know mass and length is dropped from a known height and makes an impact with a notched sample. The pendulum fractures the sample upon impact and continues its swing, but it does not reach the same height as its starting position. The energy absorbed by the material is deduced from the difference in heights of the pendulum (Fig. 10). Examining the way, the material breaks gives information about the ductility of the material. A fracture on a flat plane is indicative of a brittle material, whereas a fracture with jagged edges indicates a ductile material. It is possible for a material to be completely ductile at certain temperatures and completely brittle at other temperatures. If this is the case, then there must be a transition region between these temperature intervals where the material shows the characteristics of both ductile and brittle fracture. The temperature at which this transition occurs and how wide the transition region is depend on the type of material and the thermo-mechanical treatment it received.

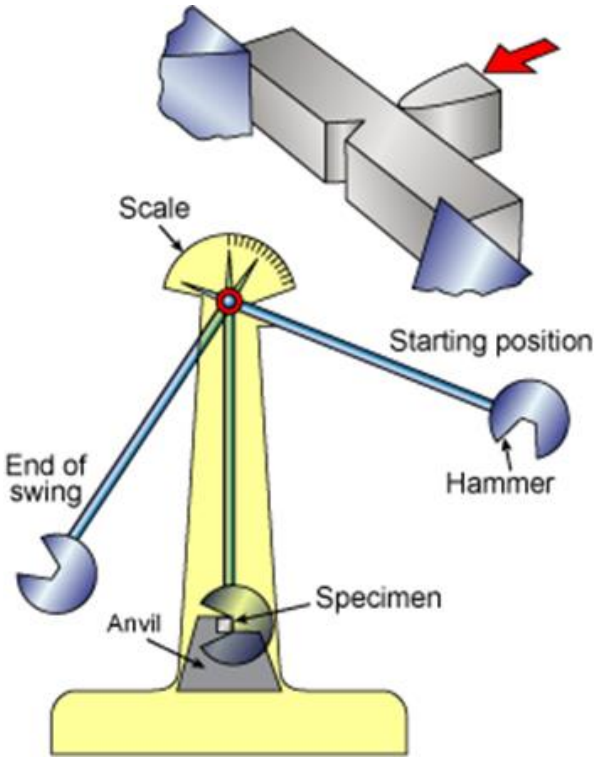

Figure 10: Schematic representation of the Charpy impact test.

3.4 Vickers hardness test

In order to perform a hardness test, a sample must be as flat as possible and free from imperfections on the surface on which the diamond press of the Vickers hardness machine pushes down. In order to achieve the desired flatness, both sides of a sample must be grinded. Following this, one side must also be polished to remove scratches caused by the grinding. Grinding is performed by gluing a sample onto a holder and pressing it against a spinning SiC disc. The roughness of such a disc is defined by its grid size and density, a lower number corresponds with a rougher surface. The materials tested in this thesis are grinded with the following grid sizes and densities: 500, 1200, 2000 and 4000 grid, all applied in this specific order. Polishing one of the grinded surfaces of the sample removes its scratches. An abrasive fluid with particles of known size is applied to the spinning disc. In this thesis, the samples are first polished with 3 µm

particles solution followed by another polish with 1 µm particles solution. This process is completed once all scratches that were visible by the naked eye are removed.
Optionally, one can polish a sample further applying electrolyte polishing. However, early test with this process showed a tendency to apply a metal coating to the sample which is unfavourable for this research. Hence, it was chosen not to perform the electrolyte polishing on any of the samples.

The Vickers hardness test observes the material's ability to resist plastic deformation when a known force is applied. This is a very general hardness test, as it can be used for all metals and covers a wide hardness scale. The test consists of pressing a square shaped diamond into the sample and measuring the length of the diagonals of the indentation. The angle from each face normal to the horizontal plane is typically 22°. The hardness is given in a unit known as the Vickers Pyramid Number (HV) and is the ratio of the applied force over the area of the indentation. The area A is calculated with the following formula [25].

$$A = \frac{d^2}{2 \cdot \sin\left(\frac{136°}{2}\right)} \tag{4}$$

or

$$A \approx \frac{d^2}{1.8544}, \tag{5}$$

where d is the average length of the diagonal of the indentation in millimeters. Hence,

$$HV = \frac{F}{A} \approx \frac{1.8544 \cdot F}{d^2} \qquad \left[\frac{kgf}{mm^2}\right] \tag{6}$$

where F is the applied force in kilogram-force (1 kgf = 9.81 N).
A common application of the hardness test is not to derive engineering properties, but rather to use it as a quick and non-destructive way to gauge the yield strength and how much greater the ultimate tensile strength is (providing a measure for the work hardening). A general rule of thumb is that the yield stress of an alloy in MPa is roughly equal to three times its hardness in HV [26]. Also, the difference between the yield and ultimate tensile strength is proportional to the change in hardness between a regular material sample and one that experienced plastic deformation. Having a general idea of what values to expect from the tensile test can prevent situations where it is applied outside the ductile regime, rendering the test useless.

3.5 Tensile test

The tensile test subjects a sample to controlled tension until the material fractures. From this process, the Young's modulus, Poisson's ratio, yield strength and work hardening can be deduced. The elongation of the material is compared to the applied force. With this, the engineering strain can be calculated.

$$\varepsilon = \frac{\Delta L}{L_0} \tag{7}$$

Here, ΔL is the change in length and L_0 is the initial length of the sample. Furthermore, the engineering stress is recorded during the test.

$$\sigma = \frac{F}{A} \tag{8}$$

F is the applied load and A is the area of the cross-section of the sample. The difference between engineering stress and true stress is that for the calculation of engineering stress, the cross-section of the

sample is equal to its initial cross-section and assumed to be constant during the whole test. The true stress considers the reduction in cross-section due to necking. Most stress-strain curves depict the engineering stress (Fig. 11).

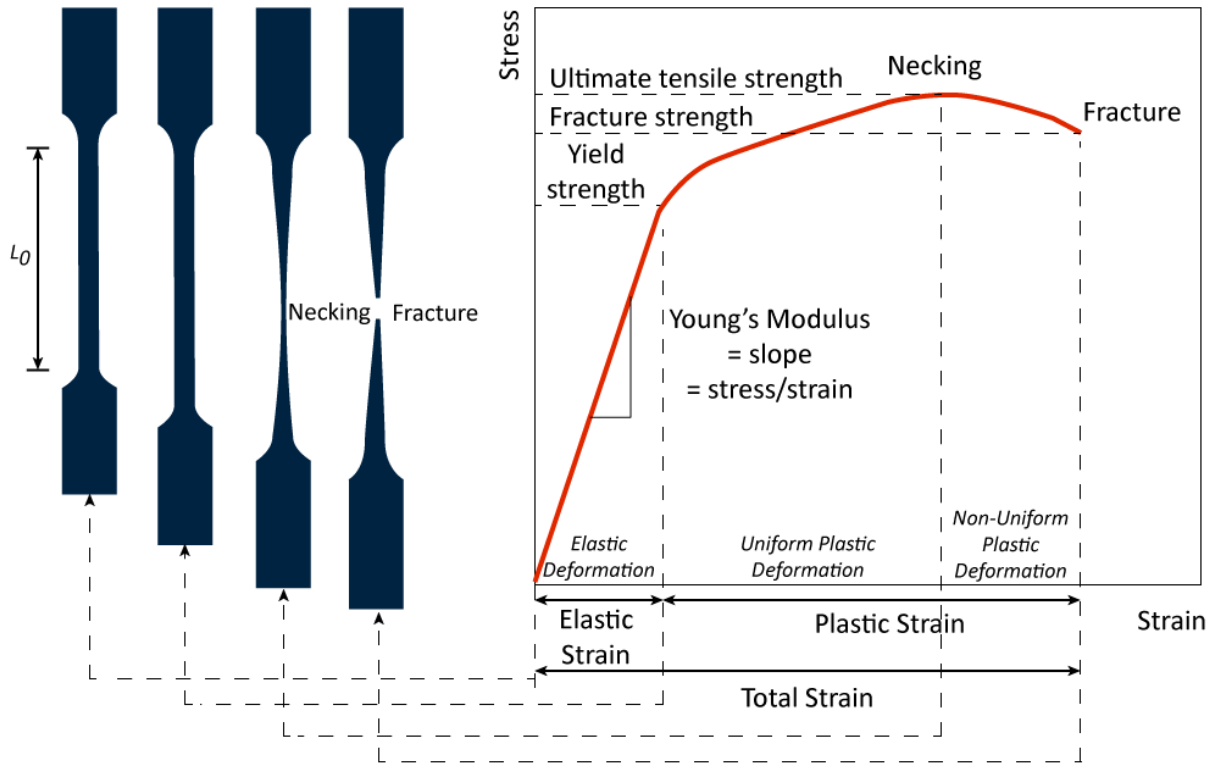

Figure 11: Geometry of a tensile test sample and an example of a (engineering) stress-strain curve [27].

4 RESULTS AND DISCUSSION

4.1 Scanning electron microscope

The fracture surfaces of two samples of regular Eurofer97 from a series of Charpy impact tests were examined using a scanning electron microscope (SEM), one was broken at -175°C and the other deformed at room temperature.
In a brittle material, a fracture propagates along a path of weakness produced by either microstructural variables or a reactive environment. This path is often defined by the grain boundaries of the material, which can be weakened in several different ways. When a fracture propagates in this way, the fracture surface shows a definite intergranular appearance (Fig. 12) [28, pp. 49-51].

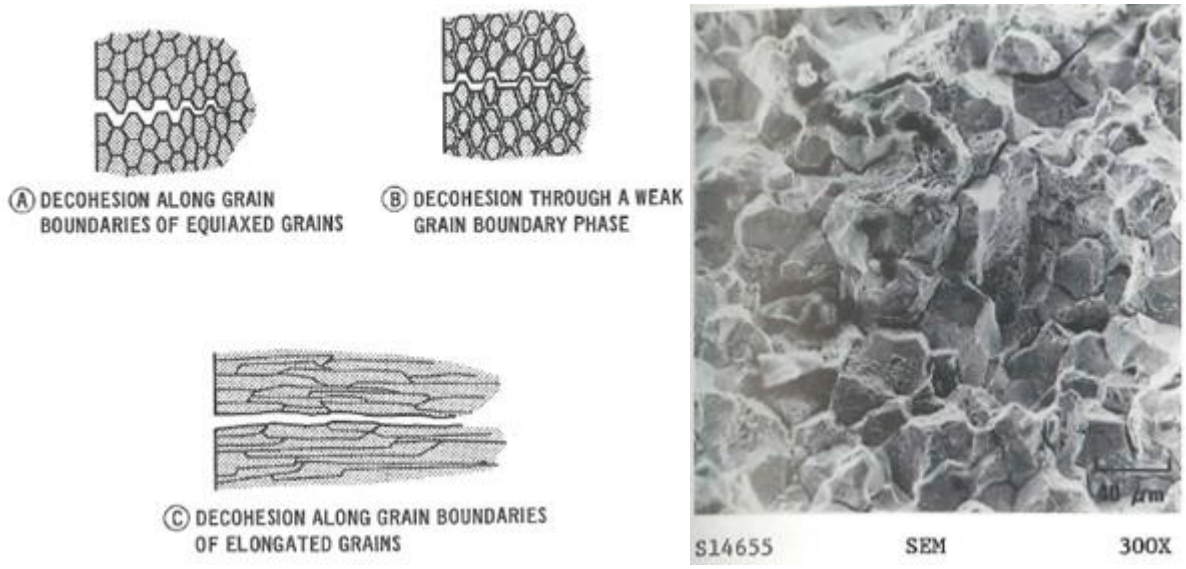

Figure 12: Fracture propagation along grain boundaries and the resulting intergranular appearance [28, pp. 50-51].

The Eurofer97 sample that was cooled to -175°C does not display this ‘rock-candy’ like appearance of intergranular fracture (Fig. 13). Rather, it appears that the path of weakness in this material does not follow the grain boundaries, instead preferring to cut through the grains. This is called transgranular fracture and is common in most modern steels due to the limited amount of weakening of the grain boundaries. Transgranular fracture can only be the main type fracture in a metal if it experiences fully brittle fracture, meaning its temperature was below the DBTT.

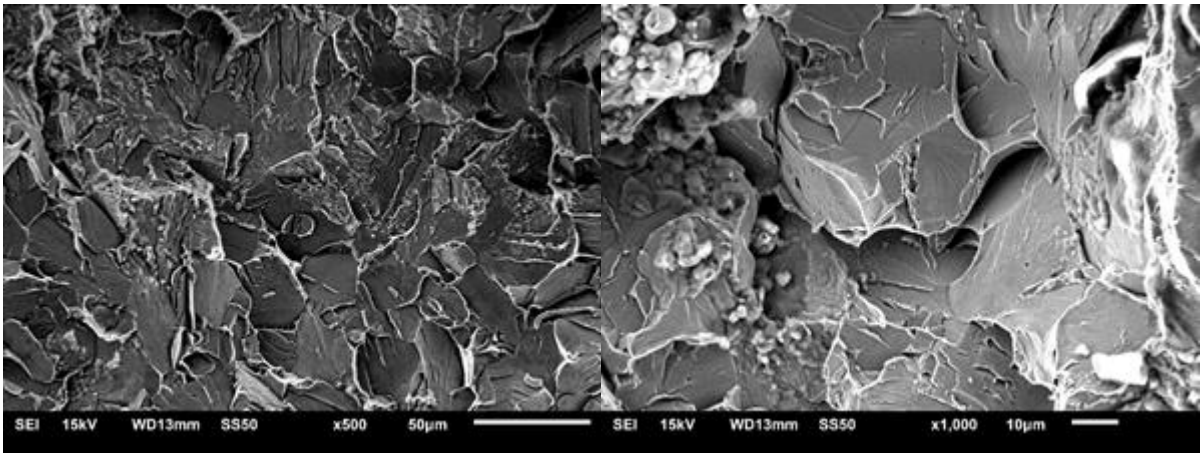

Figure 13: SEM picture of Eurofer97 fracture surface at -175°C. Magnification of 500 (left) and 1000 (right).

Looking at the fracture surface of the sample deformed at room temperature through SEM shows a very different behaviour than the previous sample. Rather than breaking, the impact of the hammer caused the V-notch at the opposite side of the impact to tear open the sample. A material can be torn open due to the nucleation of microvoids at areas of localized high plastic deformation. As the load on the material increases, these microvoids grow and start to coalesce until they eventually form a continuous fracture surface. The microvoids leave behind cup-like depressions referred to as dimples (Fig. 14) [28, pp. 25-26].

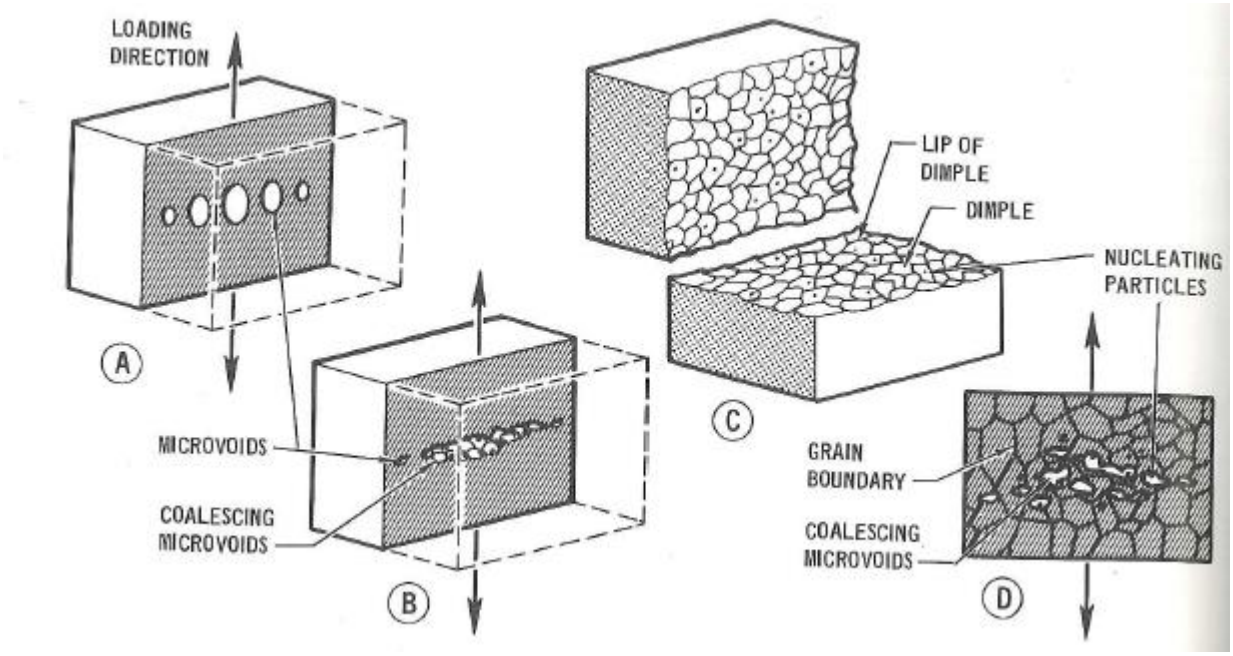

Figure 14: Dimple formation by microvoid coalescence.

The type of stress experienced by the material strongly influences the shape of the dimples. As mentioned before, this fracture surface was created by tearing the sample open, leaving behind elongated or parabolic dimples. In case of tear fracture (in contrast to shear fracture), the dimples on both fracture surfaces are oriented the same way, pointing back to where the fracture originated (Fig. 15-16) [28, pp. 30]

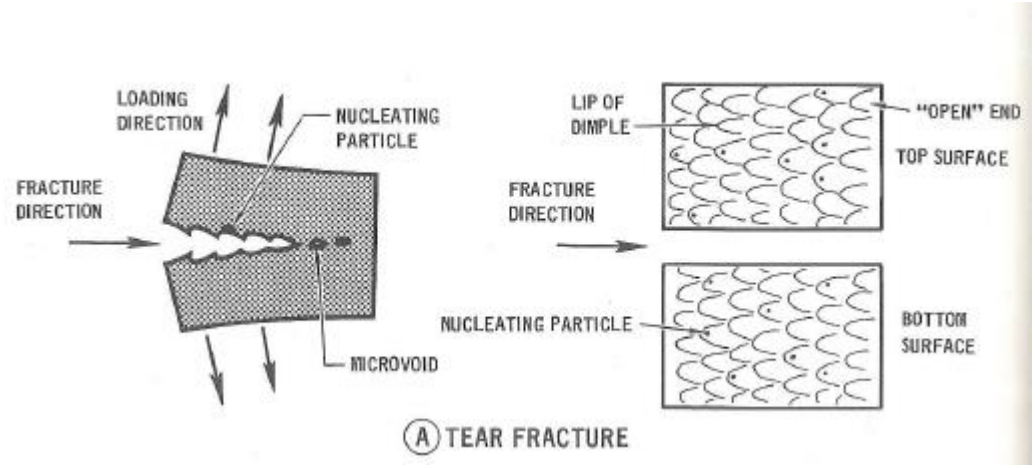

Figure 15: formation of elongated dimples under tear loading conditions.

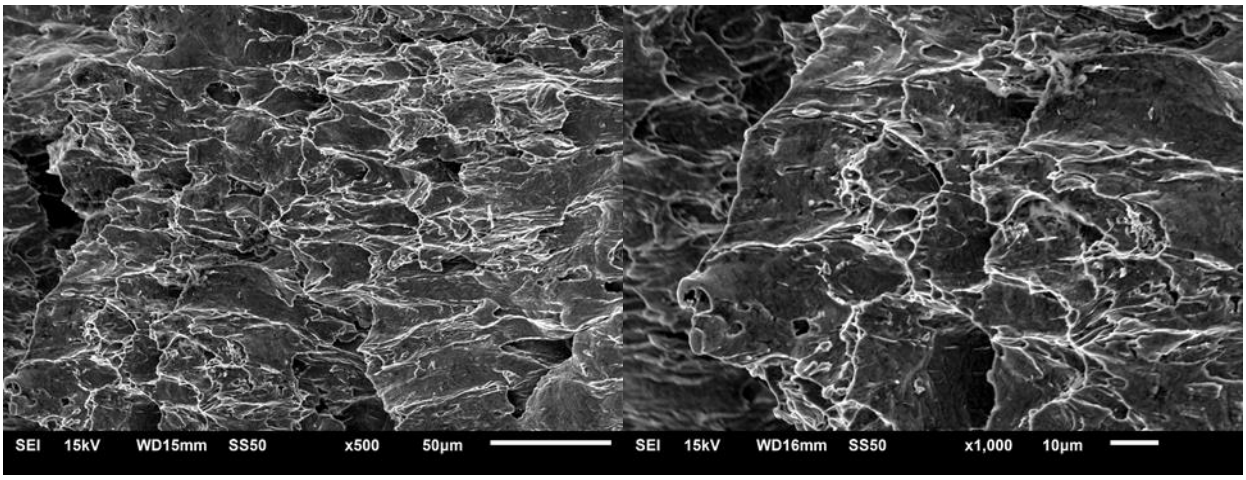

Figure 16: SEM picture of Eurofer97 fracture surface at room temperature. Magnification of 500 (left) and 1000 (right).

4.2 Charpy impact test

Charpy tests were performed on the lab-cast Eurofer at temperatures ranging between -175°C and room temperature with a hammer that carried 15 J of energy. This material shows a very sharp transition from brittle to ductile around -125°C. Samples that broke completely could only absorb a small amount of energy indicating brittle fracture. Samples that deformed, rather than broke, absorbed far more of the hammer's energy. The measurement of the absorbed energy is shown in Figure 17 along with a fit according to the following formula:

$$E = \left(L + \frac{D}{2}\right) + \frac{D}{2} \cdot \tanh\left(\frac{T - T_0}{C}\right) \qquad (9)$$

In this formula, L is the lower shelf energy (0.20 J), D the difference between upper and lower shelf energy (10.25 J), T the temperature, T_0 the DBTT and C a constant defining the slope of the transition region. Since the transition is very swift, $C = 1$ was chosen [29].

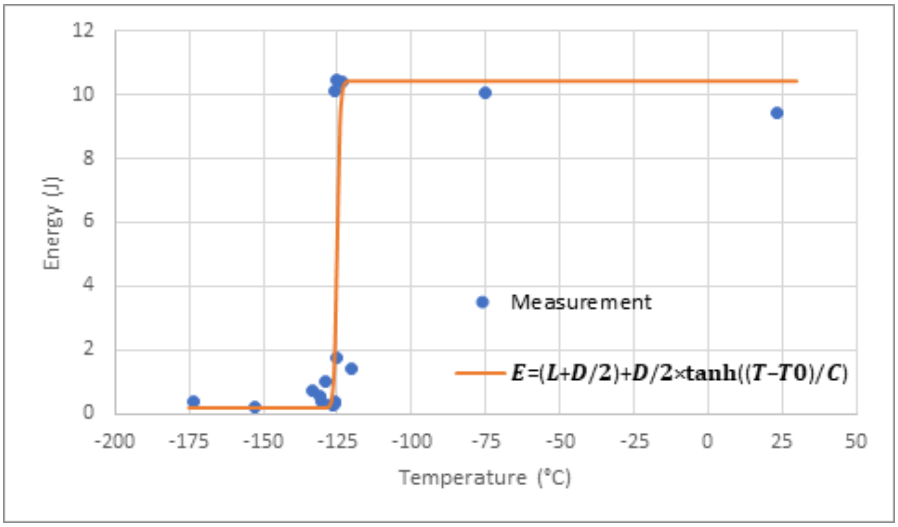

Figure 17: Energy to temperature measurements from Charpy test with fitted curve

Having concluded that there is a very sudden transition from ductile to brittle fracture, there is still a subtle difference between fractures far away from the DBTT and near it. Figure 18 depicts the force vs time curves of two samples that did not break, yet both samples behave slightly differently. The sample at DBTT (green) takes a larger initial force and thereby absorbs a significantly larger amount of energy in the first 2 ms than the sample at room temperature (blue). Taking a large initial force and most energy very quickly is exactly what a brittle sample would do, implying that the sample at DBTT is indeed in transition towards becoming brittle.

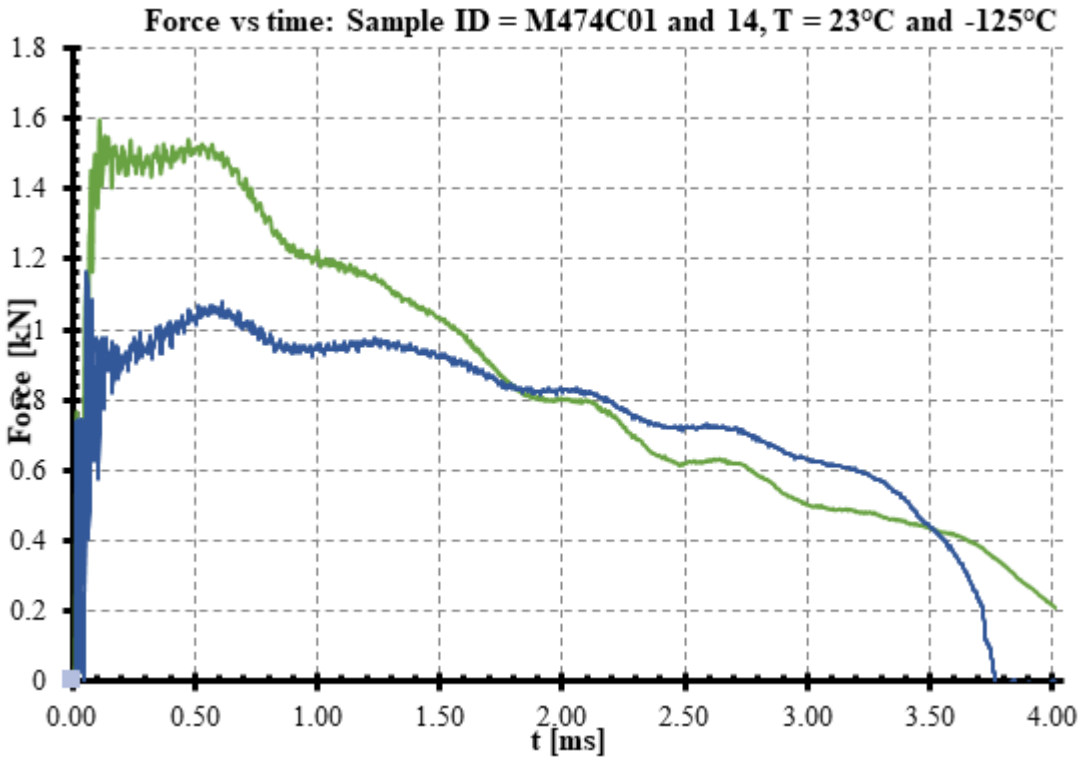

Figure 18: Charpy test at room temperature (blue) and at DBTT (green). Both samples did not break.

In a similar manner, one can look at samples that did break. Figure 19 shows the force vs time curves of two samples that broke, one at -175°C (blue) and one at the DBTT (green). Again, their behaviour is

slightly different. The sample at -175°C absorbs all the energy it can in an instant, but the sample at DBTT spreads the energy over a longer time, showing it is in transition towards a more ductile state.

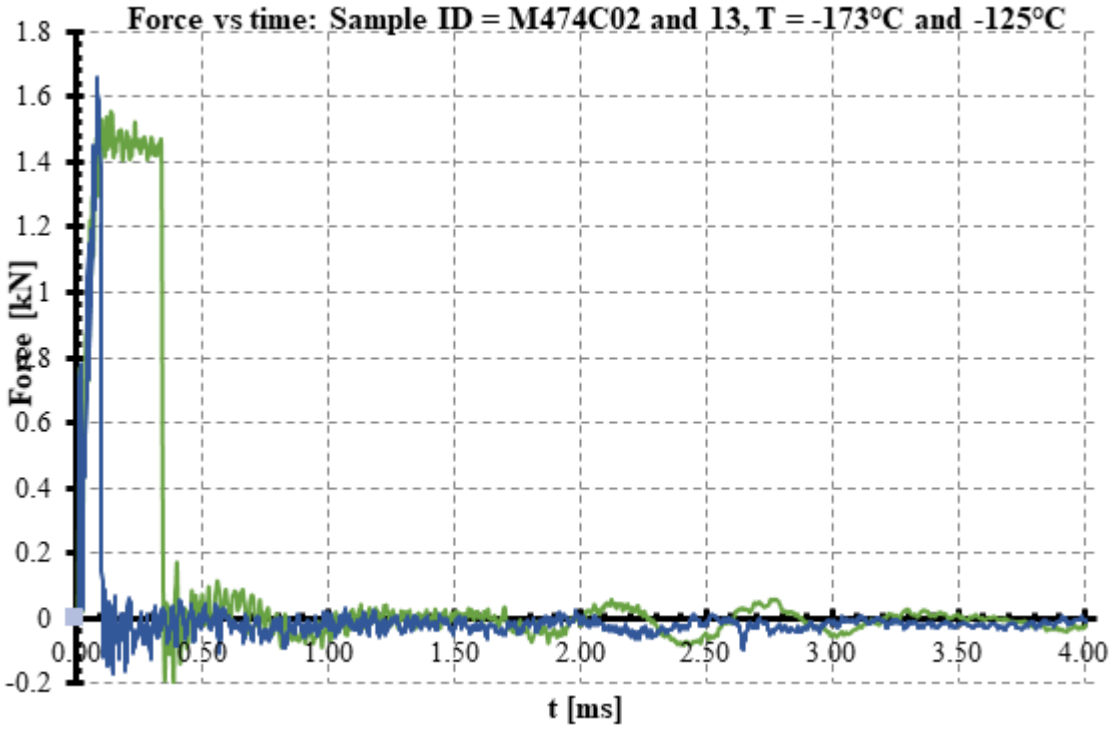

Figure 19: Charpy test at -175°C (blue) and at DBTT (green). Both samples broke.

Next to the energy to temperature curve, one can also derive information about ductility and brittleness from the lateral expansion (LE) to temperature curve. LE is the amount of width a sample gains in the direction perpendicular to the impact of the hammer during the Charpy test. The idea is that brittle materials immediately fracture, and do not get absorb a lot of energy during deformation. Ductile materials do manage to deform significantly during the test. The LE of a ductile sample is calculated by subtracting the width of the non-deformed region from the widened region where the hammer hit. The LE of a broken sample is calculated by adding together the greatest widenings in a single direction from both halves of the sample. These measurements are shown in Figure 20.

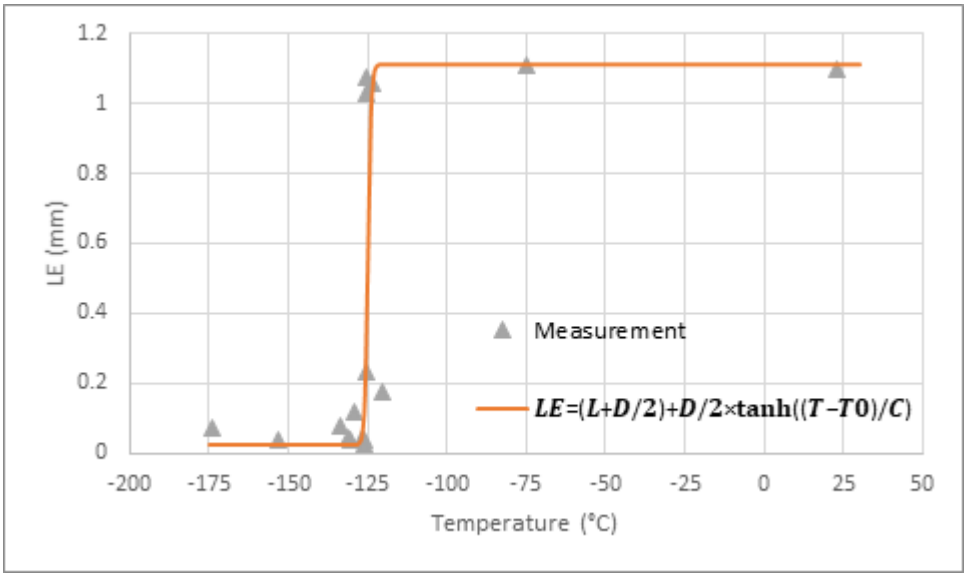

Figure 20: Lateral expansion vs temperature measurements from Charpy test with fitted curve.

The formula itself for fitting the curve remains the same as for the energy to temperature curve, only some values have changed. L, the lower shelf is now 0.026 mm, D, the difference between the upper and lower shelves becomes 1.084 mm. T, T_0 and C are unchanged. It is clear that the energy to temperature and LE to temperature curves depict the same relationship and result in the same DBTT.

Both these approaches show that the DBTT of the lab-cast Eurofer is -125°C. This is a significant change compared to -80°C, which is the DBTT of regular Eurofer97. From this, it can be concluded that the thermo-mechanical treatment the lab-cast Eurofer received has significantly improved its low temperature flow properties.

The final relation one can create from Charpy tests is the shear fracture appearance (SFA) to temperature relation. SFA is the percentage of area that has visibly experienced ductile deformation. Quantifying this number is however not always as easy. As an example, Figure 21 shows samples broken at -175°C and the DBTT. Judging from the results of previous tests, one might expect the sample at DBTT to show some faint signs of ductile fracture. On the pictures, however, it seems both samples experience completely brittle fracture.

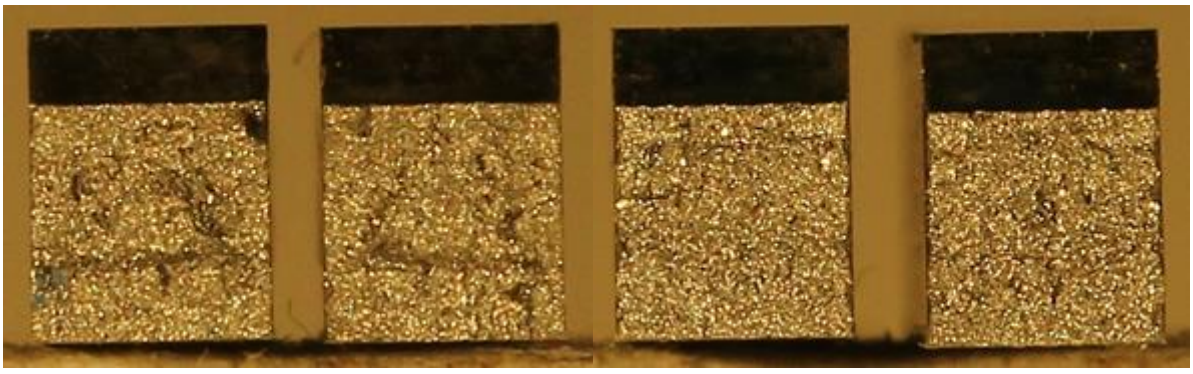

Figure 21: Cross section of brittle fracture at -175°C (left) and -125°C (right).

The ductile fractures (Fig. 22) reveal more information. Fracture at room temperature (far from DBTT) appears to be fully ductile, but at a lower temperature, a cavity starts to appear, which continues to grow

the closer the material got to the DBTT. This implies that transition towards brittle fracture does occur. Since there are samples that behaved either brittle or (mostly) ductile, both at -125°C, this method of analysing the data from a Charpy test also indicates a swift transition at a DBTT of -125°C.

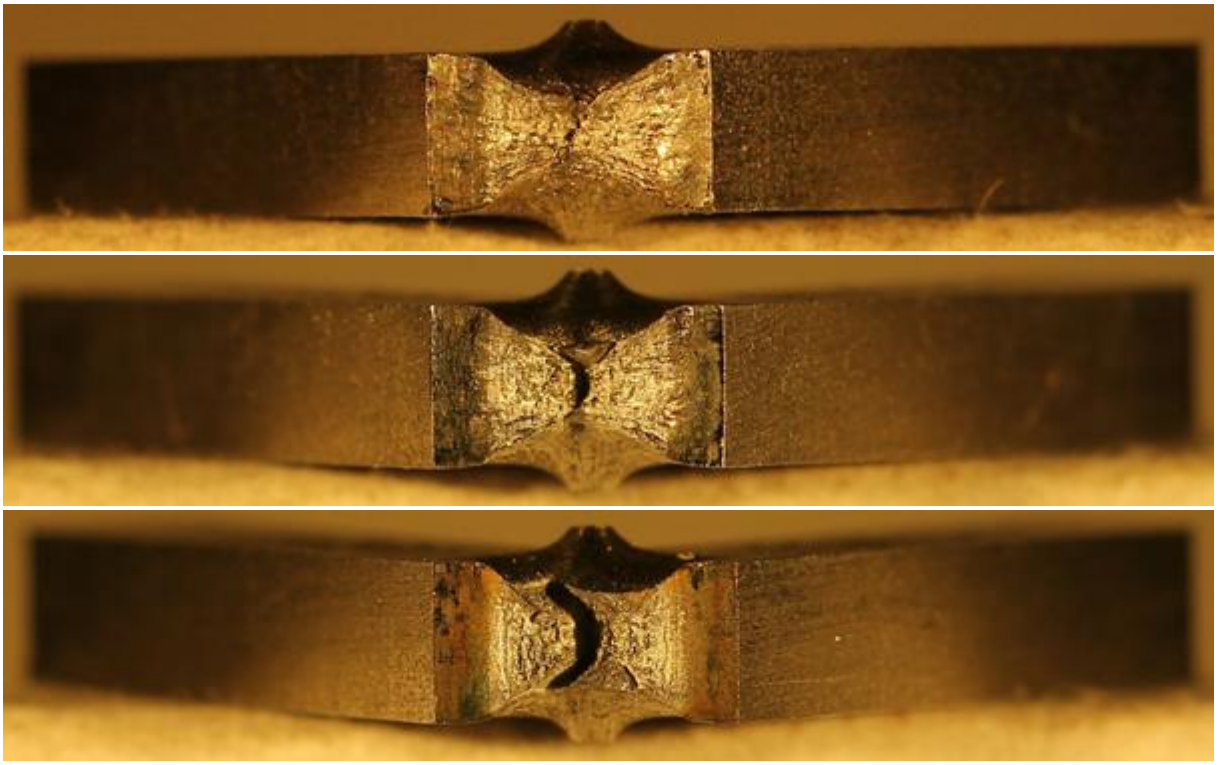

Figure 22: Ductile fracture at 23°C (top), -75°C (middle) and -125°C (bottom).

4.3 Vickers hardness test

The Vickers hardness machine can press down on the sample with different forces. For the first couple of samples, the tests were performed on CLAM steel and P91 using different forces in order to determine what force is most ideal for future tests with Eurofer grades, as these steels should have a similar hardness. The machine applies forces in multiples of 100 grams. The chosen multiples were 0.025, 0.05, 0.1, 0.2, 0.3 and 0.5. The results of these tests are shown in Figure 23.

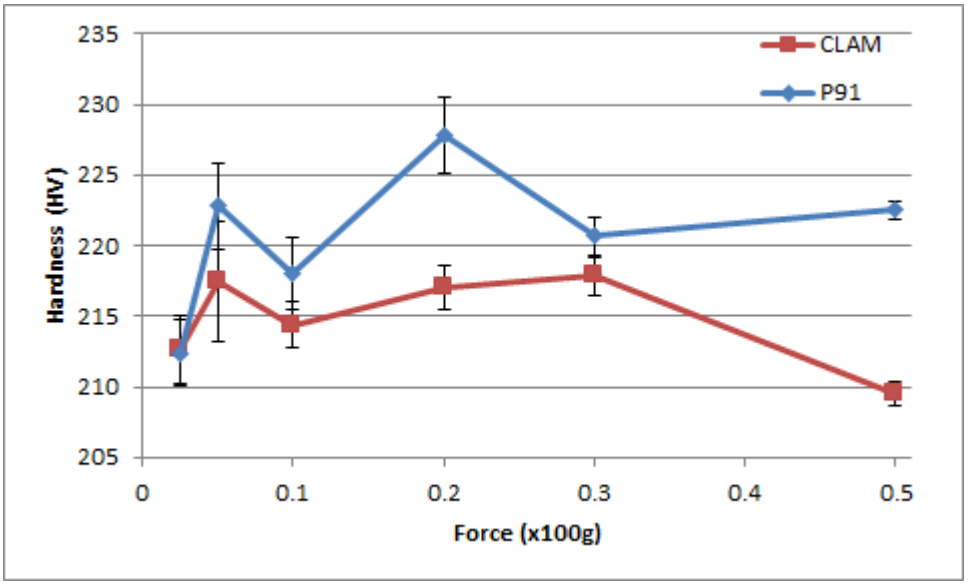

Figure 23: Hardness of CLAM and P91 steel. The error bars represent the standard error.

Ideally, the hardness obtained from these tests should be independent of the applied force, yet this seems not to be the case. A couple of conclusions can be drawn from these results. The hardness of CLAM is between 204 and 230 HV and that of P91 is around 225 HV, as expected from the literature. Performing the test with a small force (0.025 or 0.05) creates imprints that are so small that measuring the diameters of the imprint is prone to large relative deviations, resulting in a larger uncertainty in hardness of the steel. The largest force (0.5), on the other hand, has a very small uncertainty on the imprint, but it makes imprints so big that, when using the rule of thumb that an imprint causes plastic deformation in an area around itself equal to four times its diameter, the sample quickly runs out of deformable surface are, making it not ideal when testing samples with limited surface.

It is known that plastic deformation increases the hardness of a metal, the so-called work hardening. In the next series of tests, the hardness of various tungsten samples was measured, for both deformed and non-deformed sections of a flat tensile sample (Fig. 24). The two gripping areas are not plastically deformed while the thinner gauge in between is the deformed section of the sample.

Figure 24: Sketch of a flat tensile sample used in the hardness measurements.

The AL and LL tungsten samples were deformed at 300°C at 0.2 mm/min until a certain percentage of strain was achieved. The first hardness test in this series was performed on a sample of AL that experienced a strain of 8%. Because the hardness of tungsten is far greater than CLAM steel or P91, testing was again performed with different forces in order to see what effect it has on the measured hardness and determine what force to use on the other tungsten samples. The results of these measurements are displayed in Figure 25.

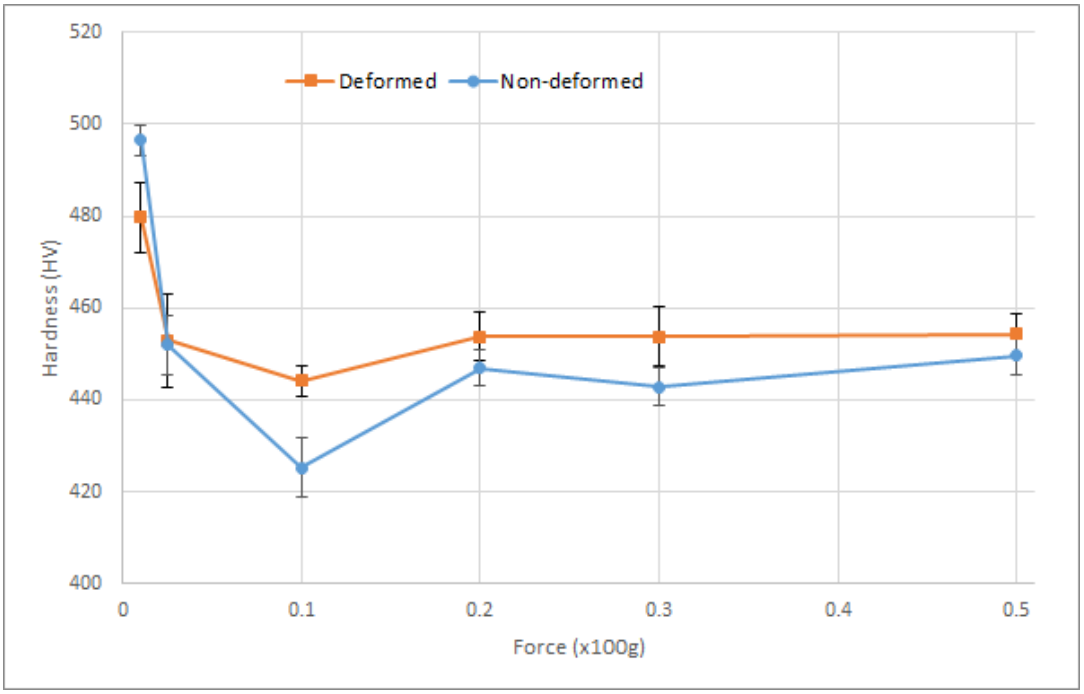

Figure 25: Hardness of deformed and non-deformed parts of AL that experienced 8% strain. The error bars represent the standard error.

Similarly to the measurements on P91 and CLAM steel, a relative force less than 0.1 gives measurements with large uncertainties and will therefore be disregarded. In this case, the deformed section of the sample has a hardness that is consistently greater than that of the non-deformed sections. The change in hardness is however quite small, ranging from an increase of 5 HV to 19 HV with relative forces of 0.5 and 0.1 respectively. These results imply that tungsten is a relatively hard material compared to other steels like P91 and CLAM steel, but not very ductile.

From these results, it was decided that a relative force of 0.2 gave the most accurate measuring results while not losing too much surface of the sample through plastic deformation, hence, the next series of hardness test were all performed with a relative force of 0.2. More samples of AL and LL with varying amounts of strain were tested this way. The effect this strain has on their hardness can be seen in Figure 26.

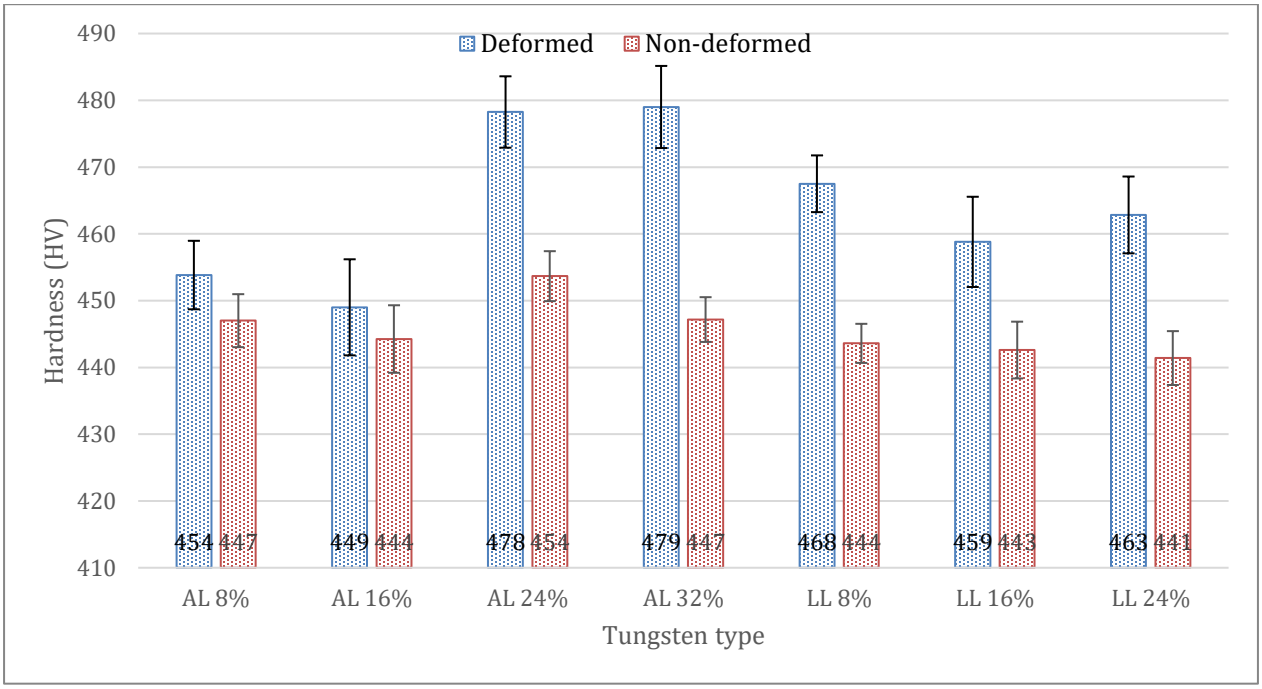

Figure 26: Hardness of deformed and non-deformed regions of various types of tungsten. The error bars represent the standard error.

As expected, the deformed sections always show a greater hardness than non-deformed sections. However, the difference in hardness between deformed and non-deformed does not simply scale linearly with the strain. Rather, it seems the increase in hardness is roughly fixed for strains above and below a critical value. AL under 8% and 16% strain get the same hardening, so do the AL samples with 24% and 32% strain. All samples of LL received comparable hardening. To explain this, one must look at Figure 27.

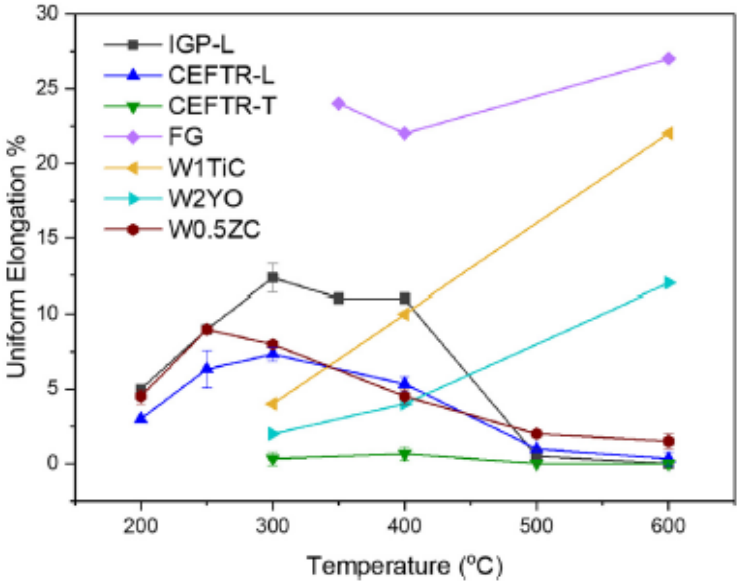

Figure 27: Uniform elongation before ultimate tensile stress is reached of a tungsten samples across various temperatures.

At 300°C, AL (IGP-L) the critical strain for uniform elongation is about 13%, which is why the samples with strains close to this (8% and 16%) behave one way, and ones with far more strain (24% and 32%)

behaved another way. All samples of LL (CEFTR-L) experienced strains above the critical strain of 7%, which is why they all experienced similar hardening.

During testing, there was one sample that defied expectations by apparently getting softer when deformed. This was the sample KL (W0.5ZC) which received 8% strain at 300°C, which is approximately equal to the critical strain seen in Figure 27. Because of this, multiple extra hardness tests were performed on the KL44 sample in order to make sure this result was consistently reproducible (Fig 28-29).

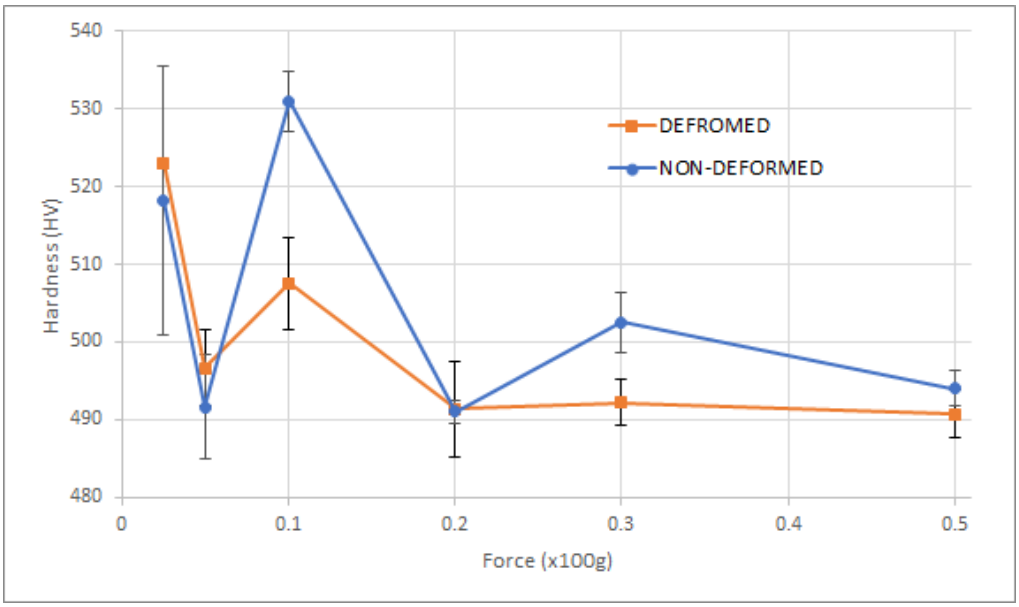

Figure 28: Hardness tests on KL 8%, series 1. The error bars represent the standard error.

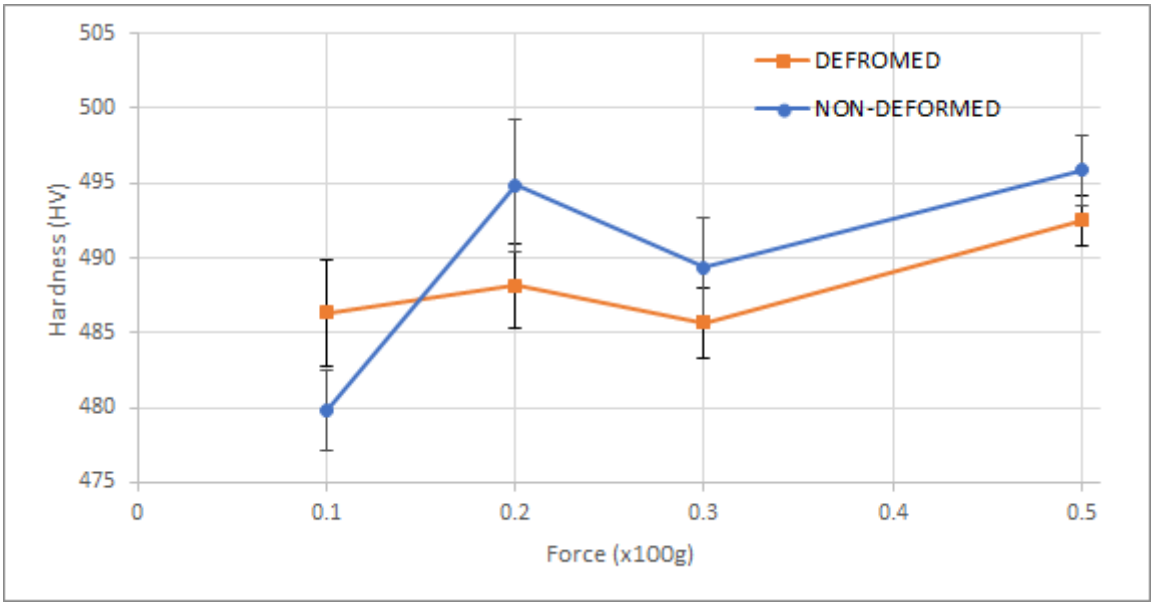

Figure 29: Hardness tests on KL 8%, series 2. The error bars represent the standard error.

The results showed consistently that, despite regular expectations, deformed KL 8% is softer than non-deformed. Upon further investigation, the reason for this is believed to be the following. The AL and LL samples were cut in a way such that their grains were orientated along the length of the sample (Fig. 30), causing the deformed section to have grains that are stretched even further. Due to the Hall-Petch

relationship, which states that the yield strength is inversely proportional to the diameter of the grains, this results in an increased hardness. KL 8% was unique in the way that its grains were oriented perpendicularly to the length of the sample (Fig. 31). This caused the grains of the deformed section to be less stretched than the regular grains, and thus effectively decreasing their diameter, leading to a decreasing hardness.

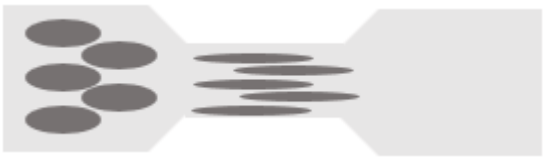

Figure 30: Sketch of regular grain orientation.

Figure 31: Sketch of grain orientation in KL44

Having seen how plastic deformation affects hardness and knowing what hardness to expect from the tests on CLAM steel and P91, the lab-cast Eurofer can be examined. The samples used for this hardness test were the same as the broken ones from the Charpy impact test. Since the shear fracture appearance did not show any signs of transition from brittle to ductile between the test temperatures -175°C and -125°C, the samples can be analysed further for signs of deformation by a hardness test. The idea is that if there is truly is no plastic deformation happening inside the brittle sample at DBTT, then the hardness should be equal when measured both close and far away from the fracture surface and also equal to the hardness of the sample broken at -175°C (Fig. 32).

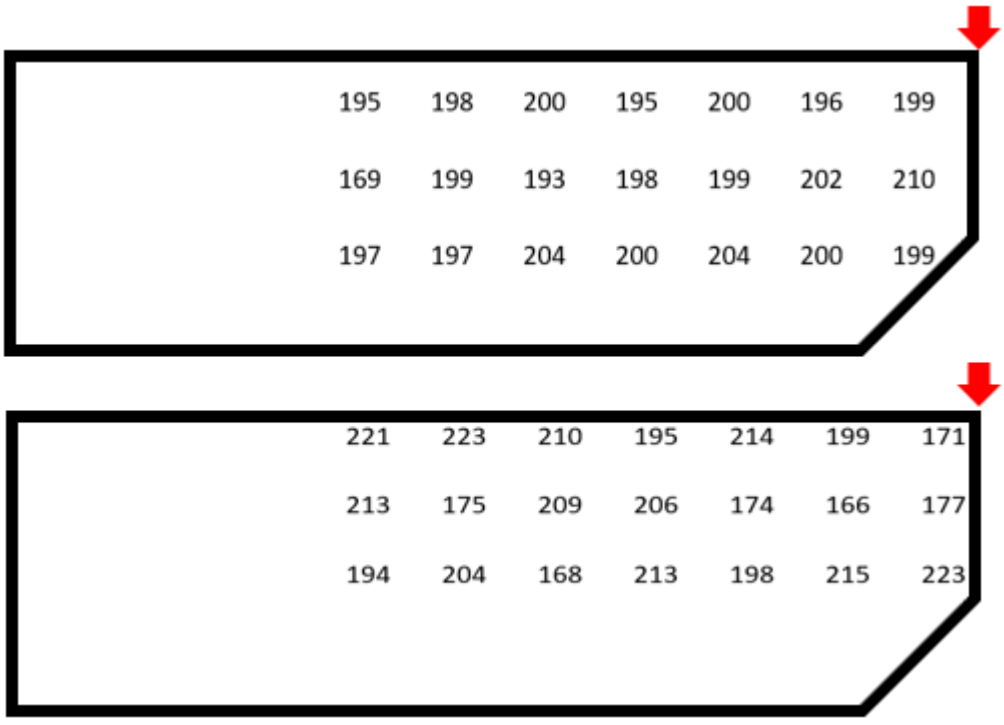

Figure 32: Hardness measurements on brittle sample broken at -175°C (top) and -125°C (bottom). The red arrows indicate the place and direction of the hammer upon impact.

The sample broken at -175°C and -125°C have an average hardness of 198.5 ± 4.2 HV and 197.8 ± 1.6 HV, which is comparable to the expected 211 HV from literature [29] and hardness of CLAM steel and P91. More importantly, if there is one area where one could possibly expect to see hardening trough plastic deformation, it would be on the very right-hand side where the fracture surface is located. Yet, the measurements indicate that there is no hardening occurring there. This method, too, shows that the fracture is completely brittle, meaning no plastic deformation happened.
When performing the same test on a flattened, deformed sample, a major increase in hardness can be seen near the location the hammer hit the sample (Fig 33). Not taking these points into account, the sample has an average hardness of 200.2 ± 3.1 HV. The plastic deformation travels far through the sample but the increase in hardness it causes diminishes quickly when moving away from the origin. The top part being sheared open has less effect on the hardness in the immediate vicinity than the bottom part being pushed into itself.

Figure 33: Hardness measurement of ductile sample, deformed at 23°C. The red arrow indicates the place and direction of the hammer upon impact.

When measuring very close to the impact point, an increase in hardness of about 70 HV is measured. Using the rule of thumb that the effect of deformation on a stress-strain curve in MPa is three times as large as the effect on hardness in HV and knowing from literature and the upcoming tensile tests that there is about a 100 MPa difference between yield strength and ultimate tensile strength, an increase of 70 HV is far too great to be considered normal plastic deformation. Therefore, this part of the sample no longer be representative of real Eurofer97 since it is plastically deformed too much. Due to the deformation its microstructure, i.e., dislocation density and possibly grain size, is no longer representative for Eurofer97.

4.4 Tensile test

4.4.1 Reference tests

First, a standard tensile test was performed on three samples at room temperature in order to obtain reference curves (Fig. 34) and as a way to practice the technique. In the stress-strain curves, certain points are indicated via coloured straight lines. The meaning of these are as follows. Orange: elastic, linear region. Green: yield strength. Blue: ultimate tensile strength. Red: fracture.

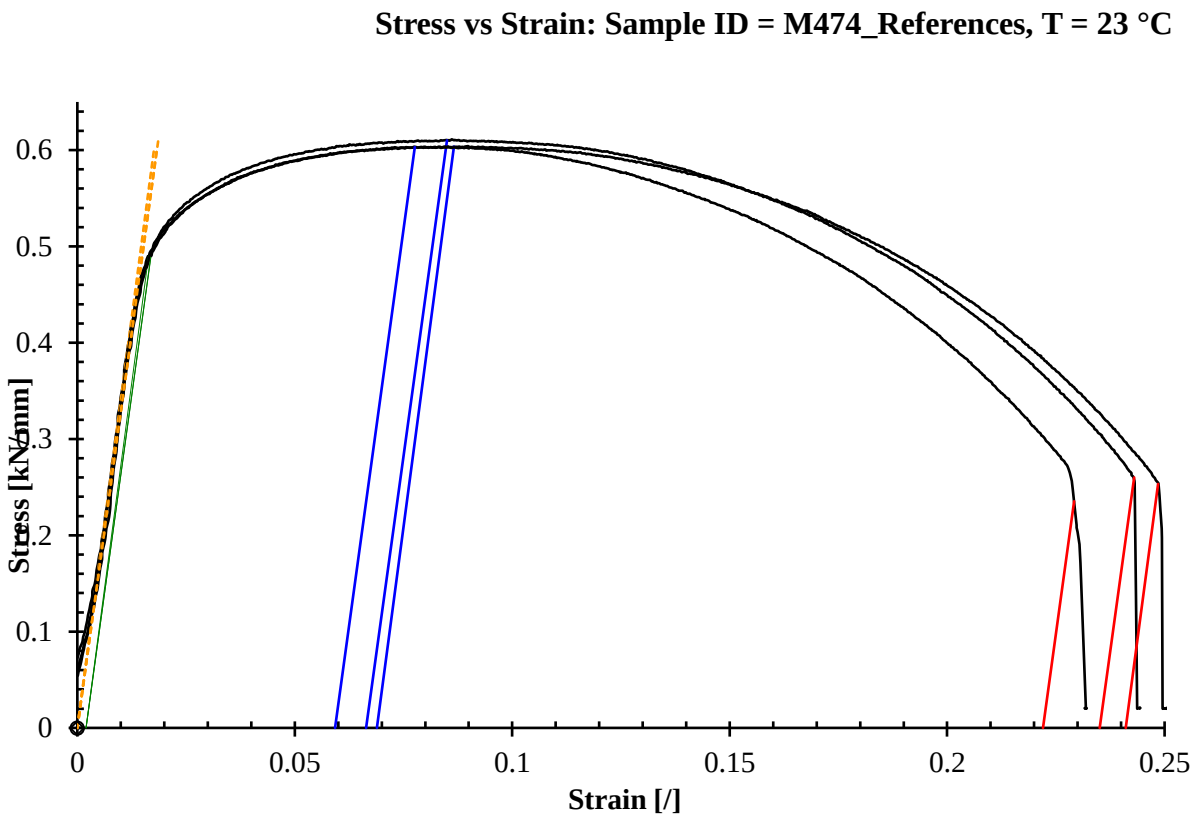

Figure 34: Stress vs Strain (References): Sample ID = M474, T = 23 °C

Another reference must be established at 300°C (Fig. 35). The effect temperature has on the material is immediately apparent when the references from different temperatures are put on the same scale (Fig. 36). The hot sample has a significantly lower yield strength and fractures under a lower strain.

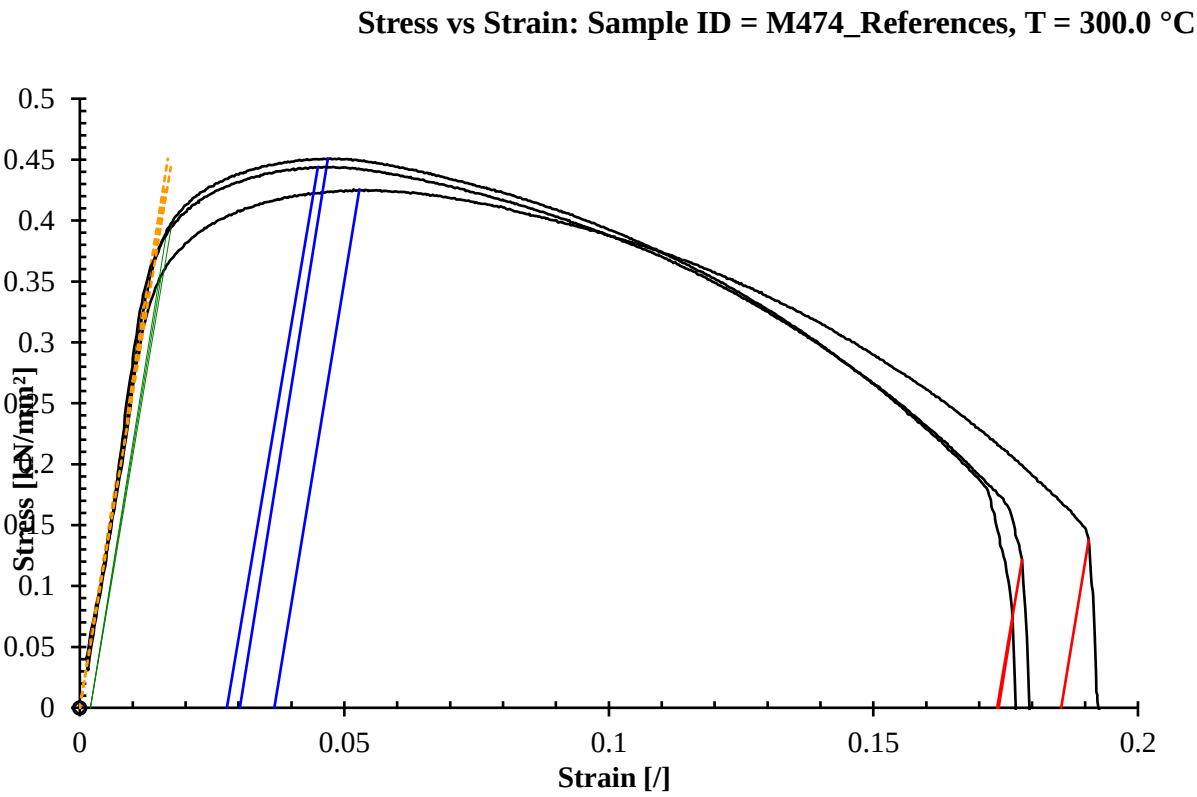

Figure 35: Stress vs Strain (References): Sample ID = M474, T = 300 °C.

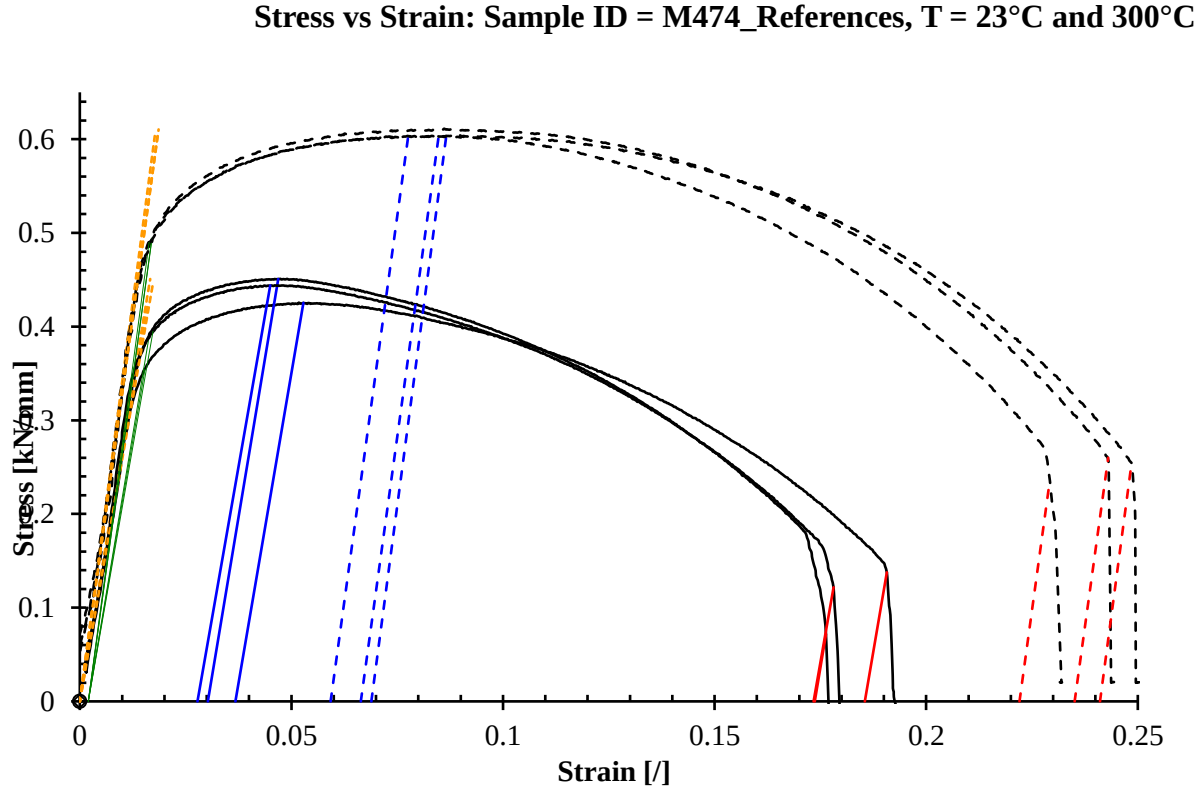

Figure 36: Stress vs Strain (References): Sample ID = M474, T = 300°C (full line) and 23°C (dashed line).

4.4.2 Validation of interrupted testing with fixed loads.

One of the objectives of this work is to reduce the number of samples needed to construct the temperature dependent yield stress curve. For this, it is necessary to check if interrupted tests produce the same stress-strain curve as a standard test. If performing interrupted tensile tests results in a stress-strain curve that differs greatly from the reference, it will not be representable for a tensile test at different temperatures to give reliable data.

On the reference curves, an interval must now be defined from the elastic limit to the yield strength. The elastic limit was chosen at the point where the derivative of the load over time reached a local maximum, after which it starts falling rapidly. This indicates the beginning of plastic deformation in the material. Using this method, the elastic limit of the sample at room temperature was reached at 1.46 kN and the yield strength of 491.0 ± 2.6 MPa at 2.234 kN. The hot sample reached its elastic limit at 1.244 kN and its yield strength of 379.3 ± 18.1 MPa at 1.723 kN.

With this, the intervals for the first series of interrupted tests are known. At room temperature, at first, the maximum load is set to the elastic limit of 1.46 kN and relaxed to 0.20 kN. Then, a new load is applied, this time the maximum force the machine applies is 1.66 kN, after which the sample is relaxed again to 0.20 kN. This process repeats with increasing maximum force until the yield strength (2.234 kN) is exceeded. Five segments of a stress-strain curve were obtained from this method which were put together to create the (Fig. 37).

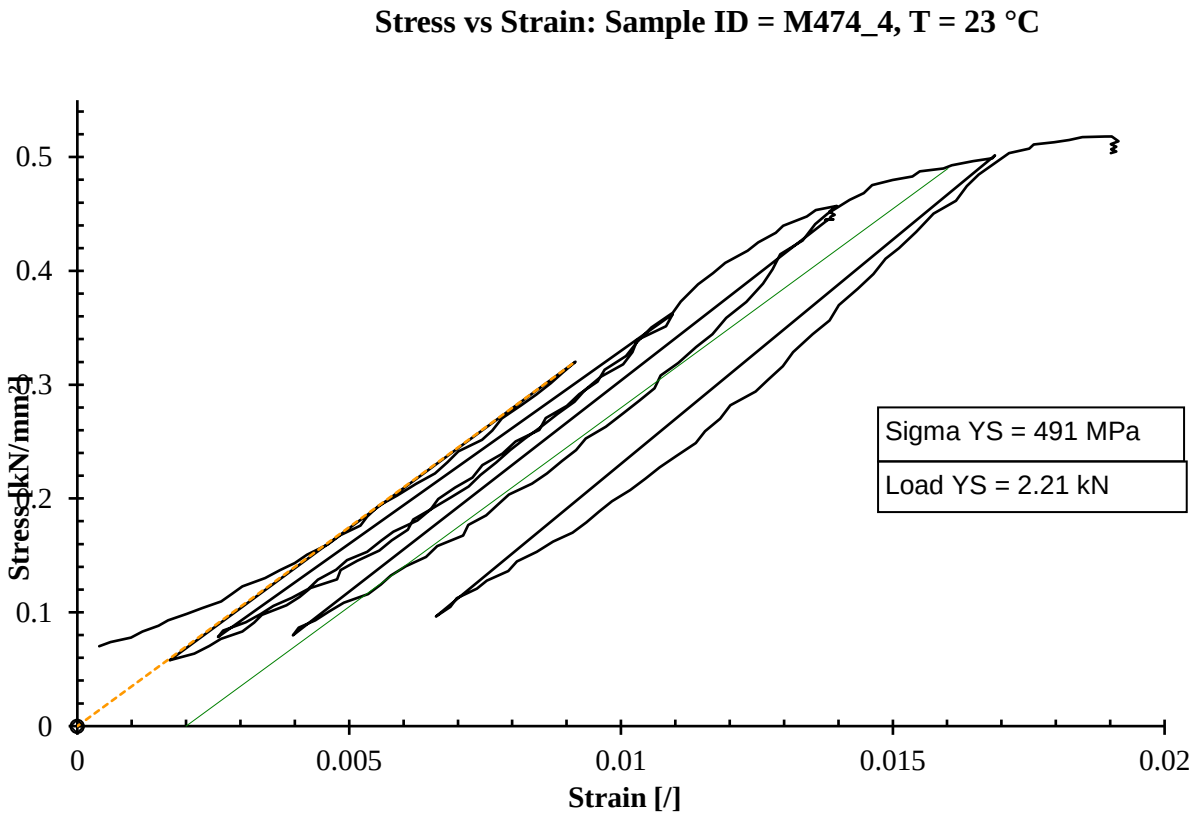

Figure 37: Stress vs Strain: T = 23 °C, interrupted tests at fixed load.

This graph gives a yield strength of 491 MPa, which is exactly what the average of the references gave. Furthermore, when this new graph is put on the same axis as the references, one can see that the results from the interrupted tests follow the behaviour of the reference curves very closely (Fig. 38). The fact that these interrupted tests preserve the behaviour of a sample that is broken without interruption means that more interrupted tests can be performed, and their results should be valid.

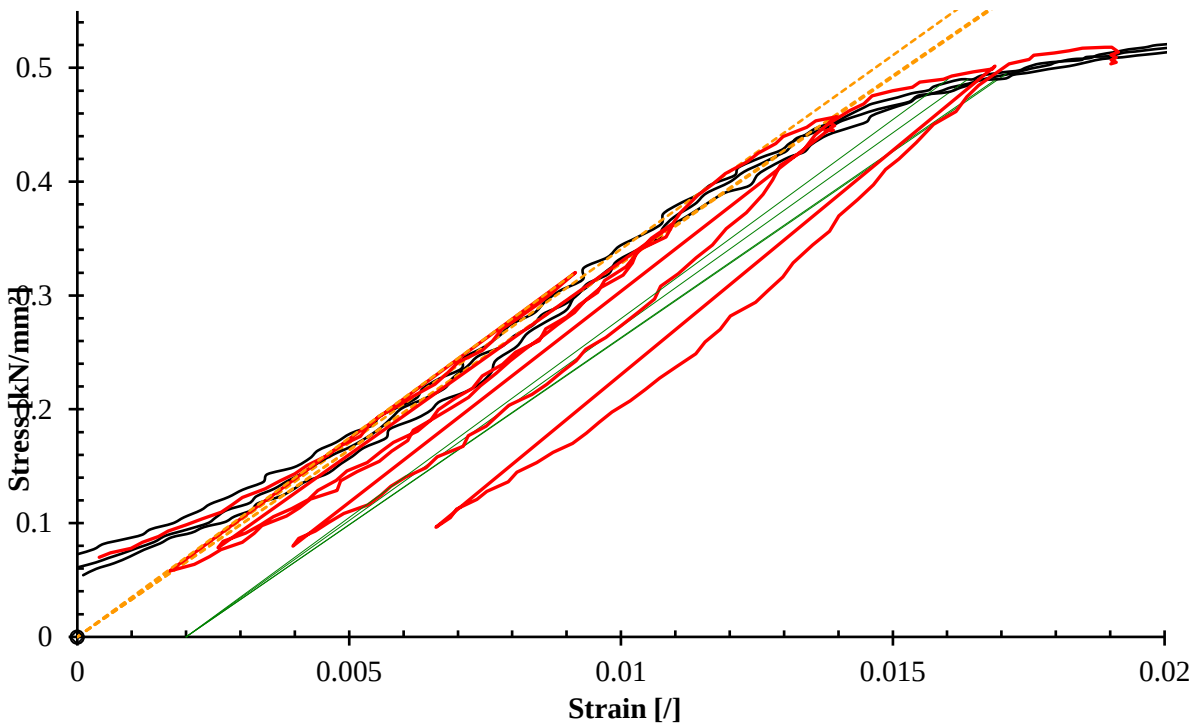

Figure 38: Stress vs Strain: T = 23 °C, interrupted tests (red) and reference graphs (black).

In a similar manner, a series of interrupted tests is done with a sample at 300°C. Its interval was determined by the reference curves to be from 1.244 kN to 1.723 kN (Fig. 39). It was then also compared to the references to verify if the interrupted procedure indeed still gives the same results as the reference (Fig. 40).

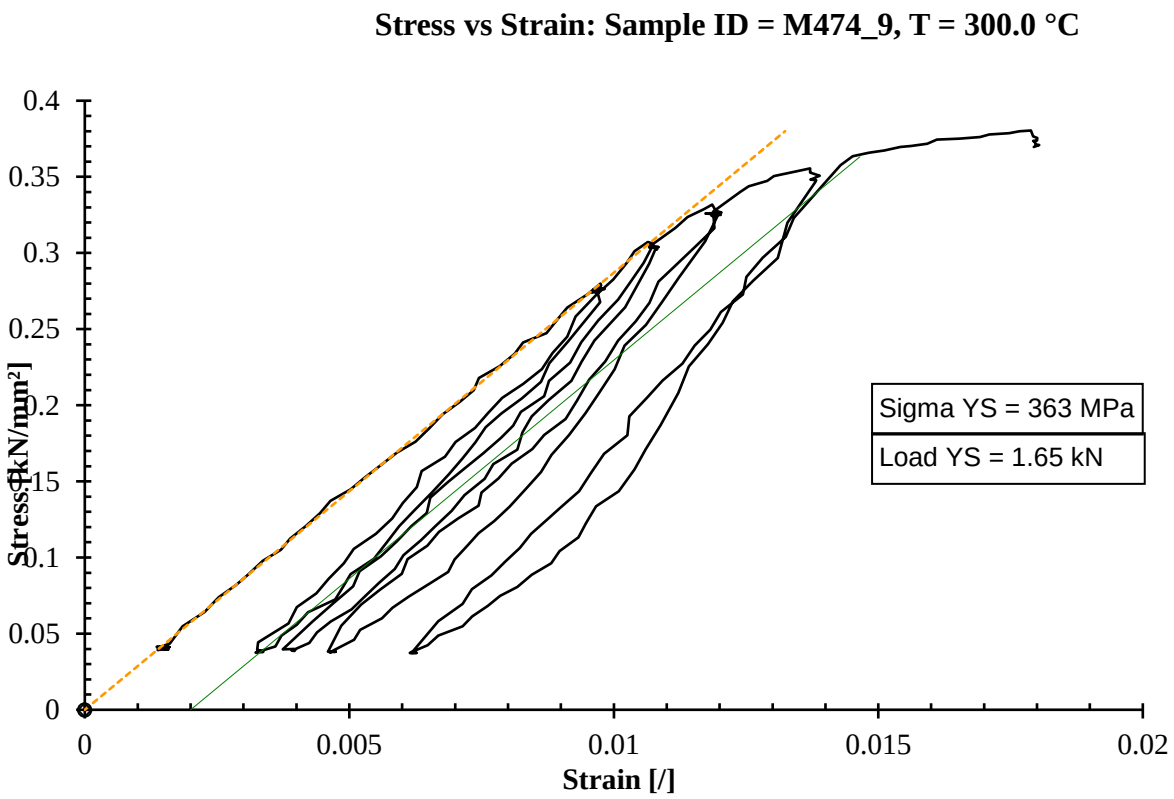

Figure 39: Stress vs Strain: Interrupted at fixed loads, T = 300°C.

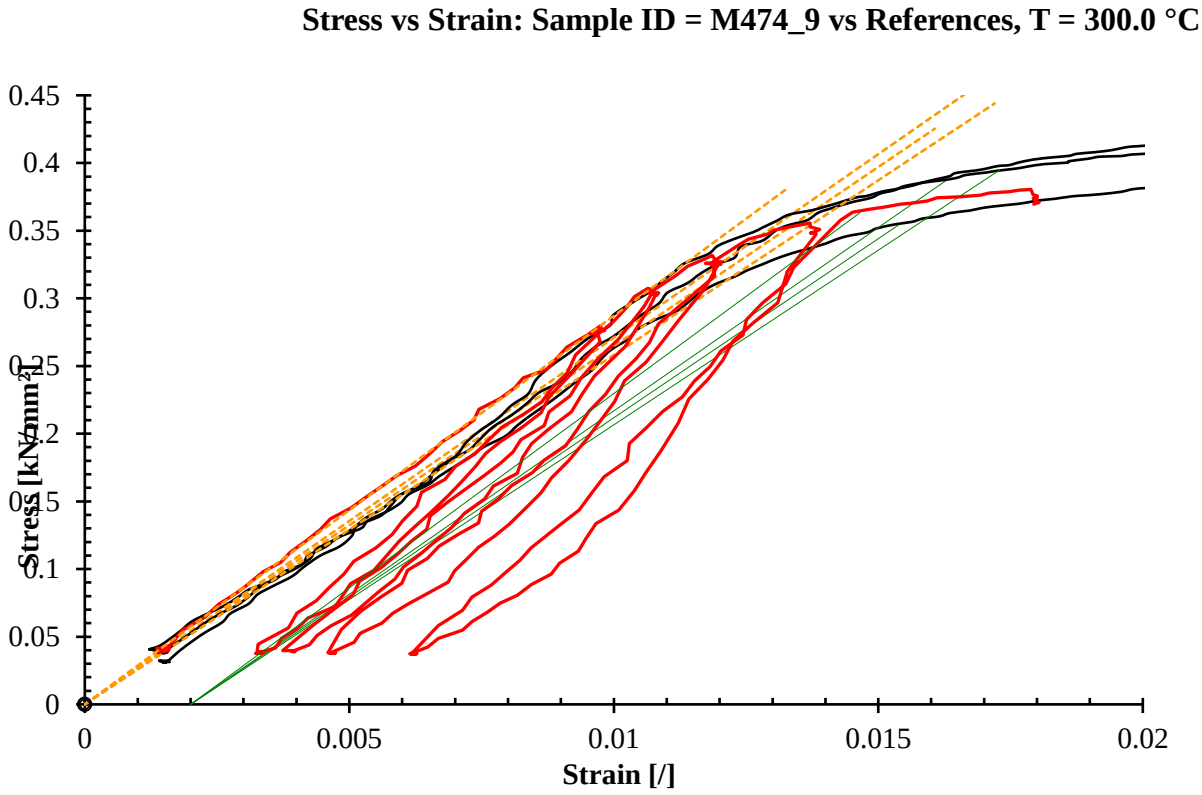

Figure 40: Stress vs Strain: T = 300 °C, interrupted tests (red) and reference graphs (black).

4.4.3 Practicing interrupted test procedure at nominal load rate

The objective now is to make another set of measurements, independent of the results obtained so far, from which one aims to derive the 0.2% yield strength of the material without needing to apply enough force to cross the yield strength. The chosen way to do this was to keep applying an increasingly higher load with a constant actuator displacement speed until a local maximal value is obtained for the derivative of the applied load over time ("load rate"), indicating the start of plastic deformation. This way, during the first couple of interruptions, the material is undergoing plastic deformation, but the load is not large enough to exceed the 0.2% strain. The complete stress-strain curve obtained this way is shown in Figure 41 and the corresponding load rate over time is shown in Figure 42 for room temperature and in Figure 43-44 for 300°C.

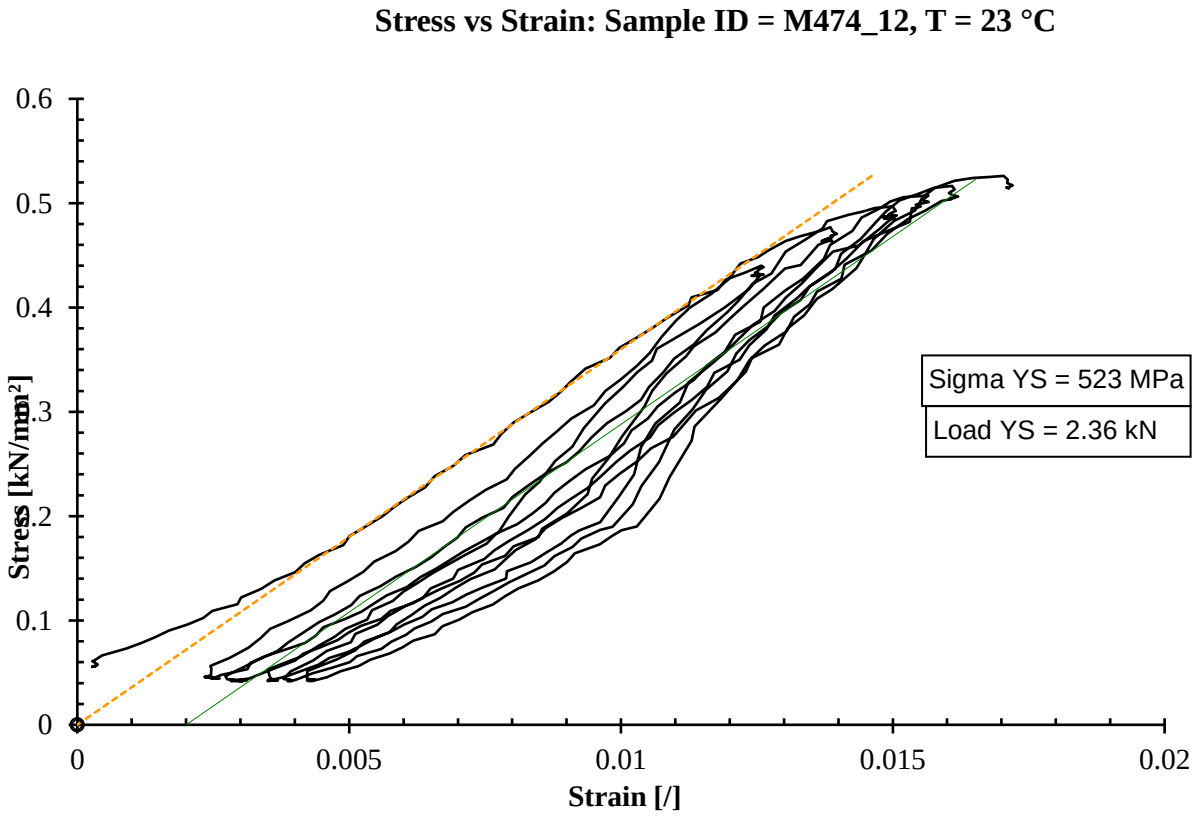

Figure 41: Stress vs Strain: T = 23°C, interrupted tests at maximal load rate.

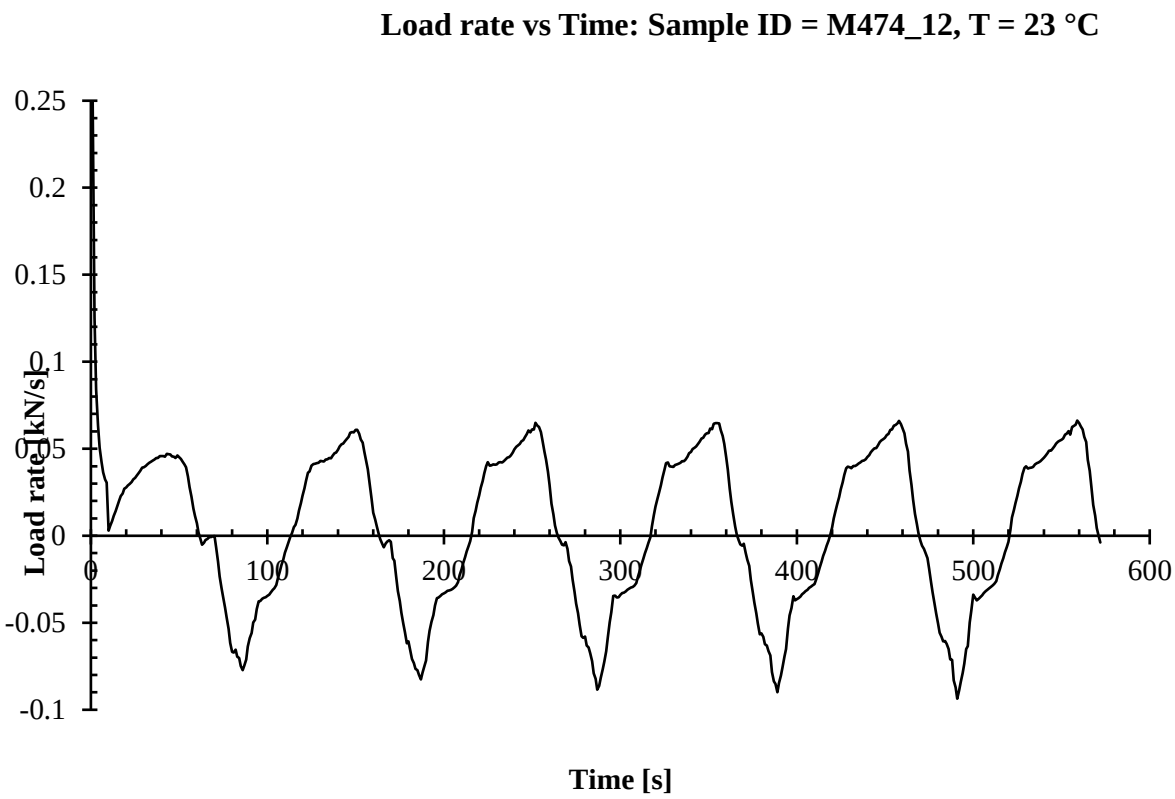

Figure 42: Load rate corresponding with Figure 41. The load is removed after reaching a local maximum.

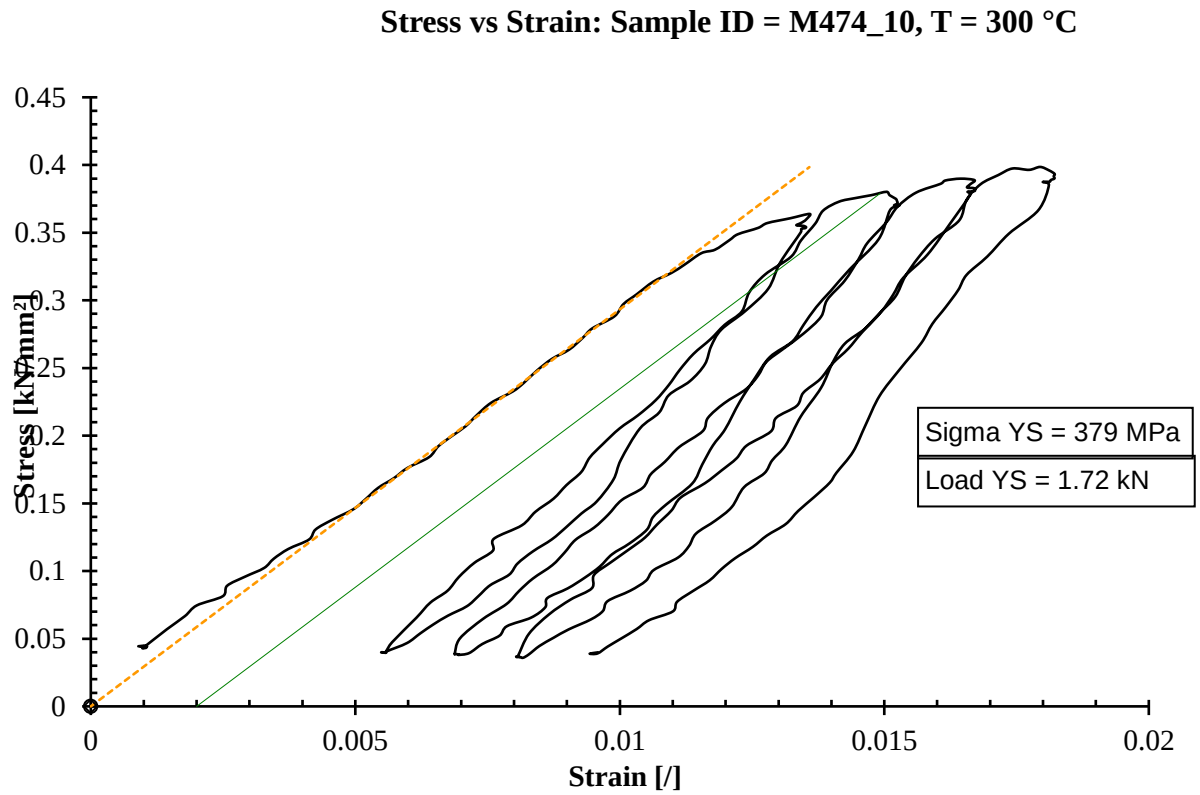

Figure 43: Stress vs Strain: T = 300°C, interrupted tests at maximal load rate.

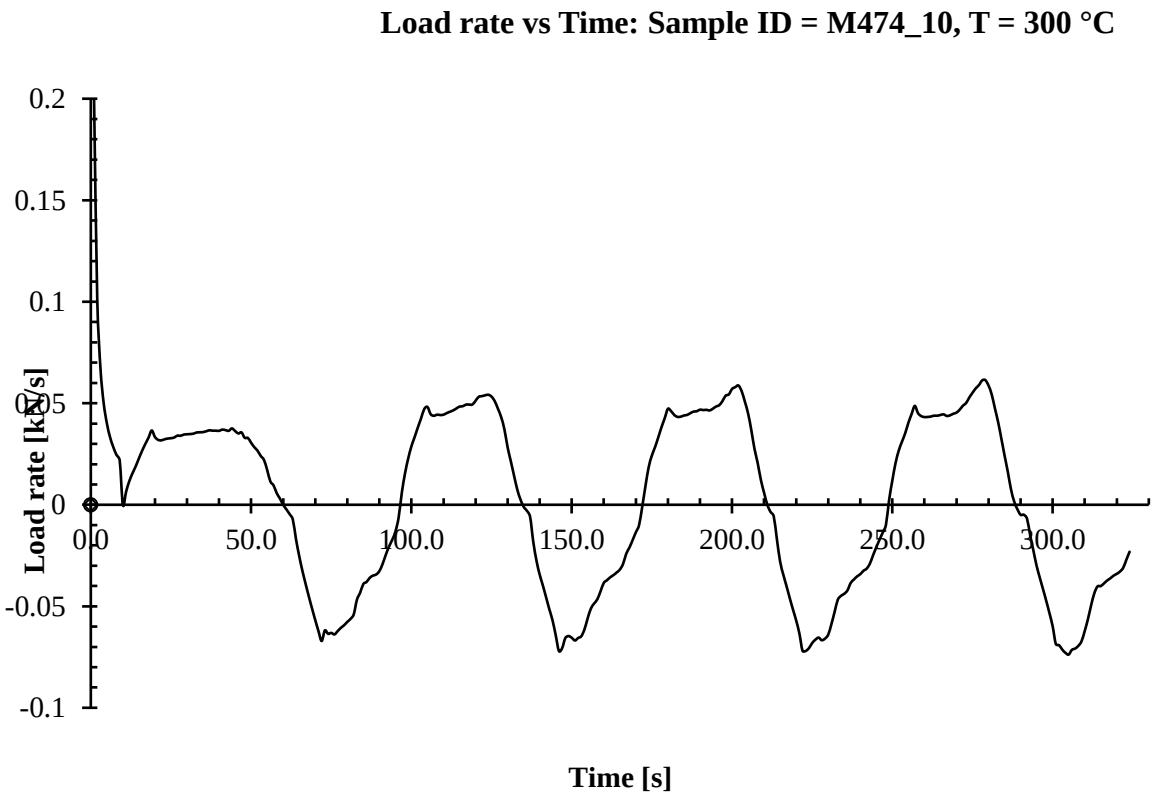

Figure 44: Load rate corresponding with Fig 43. The load is removed after reaching a local maximum.

From the data points gathered from the interrupted tests at fixed loads, trendlines are derived. Using the formulas of these trendlines and the data points obtained from the interrupted tests at maximum load rate, it is possible to calculate what the yield strength of the material should be. Since it is currently unknown what type of function gives the best fit for these curves, various functions are tested. The functions that show the most potential are linear (Fig. 45), quadratic (Fig. 46) and power functions (Fig. 47).

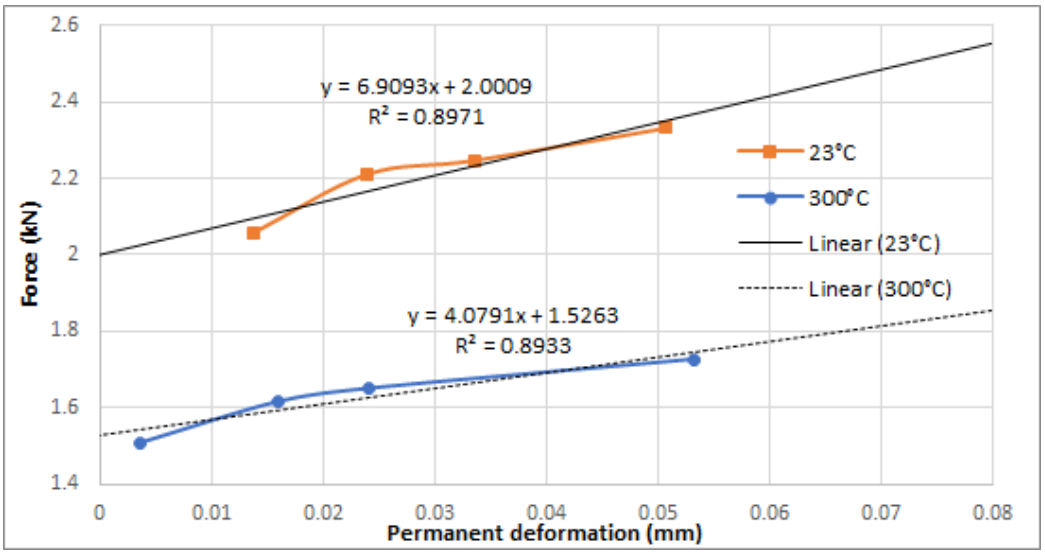

Figure 45: Data points from interrupted tests at fixed loads with linear trendline.

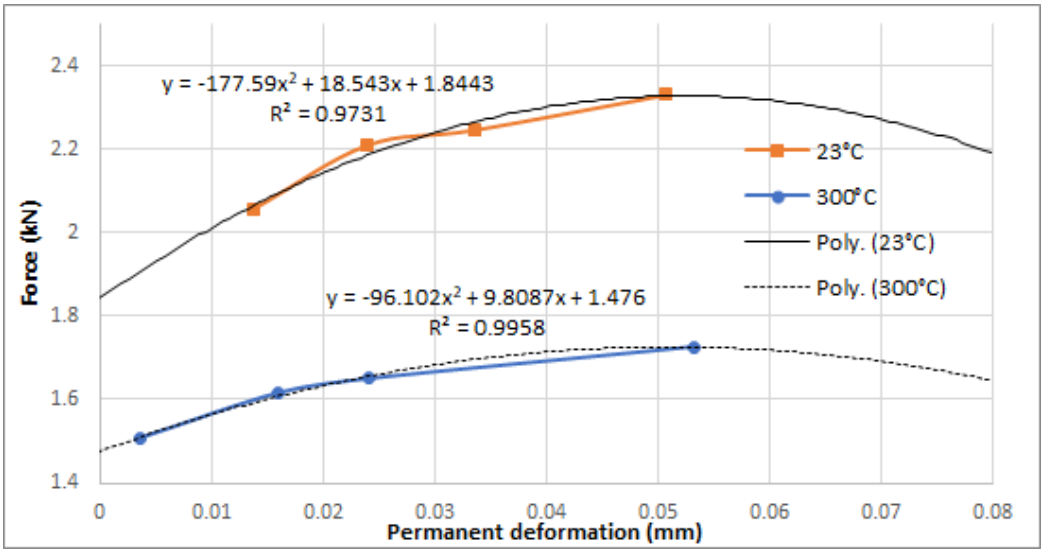

Figure 46: Data points from interrupted tests at fixed loads with quadratic trendline.

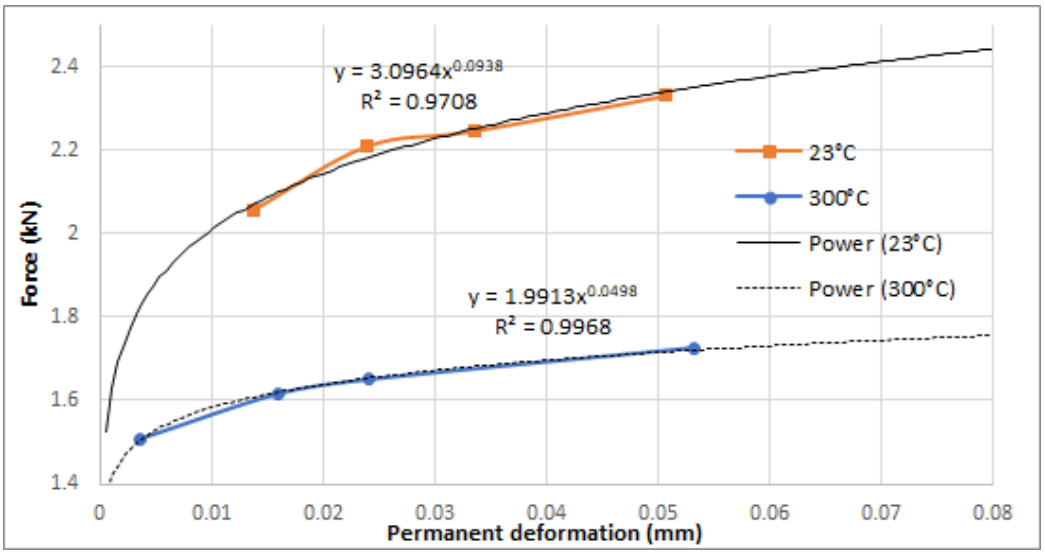

Figure 47: Data points from interrupted tests at fixed loads with power trendline.

It is important to view how accurate of an approximation of the yield strength these formulas can give. This is done as follows: a data point from the interrupted test at maximum load rate is taken and the functions in Figures 45-47 are shifted up or down such that they intersect with this point. Then the value of this shifted curve at 0.2% strain is taken. This value is the approximated yield strength.
Figure 48 and 49 show the accuracy of each type of function for 23°C and 300°C respectively by comparing the results to the yield strengths acquired from the reference curves. The more often and the further measurements are from this interval, the less accurate the approach will be considered.

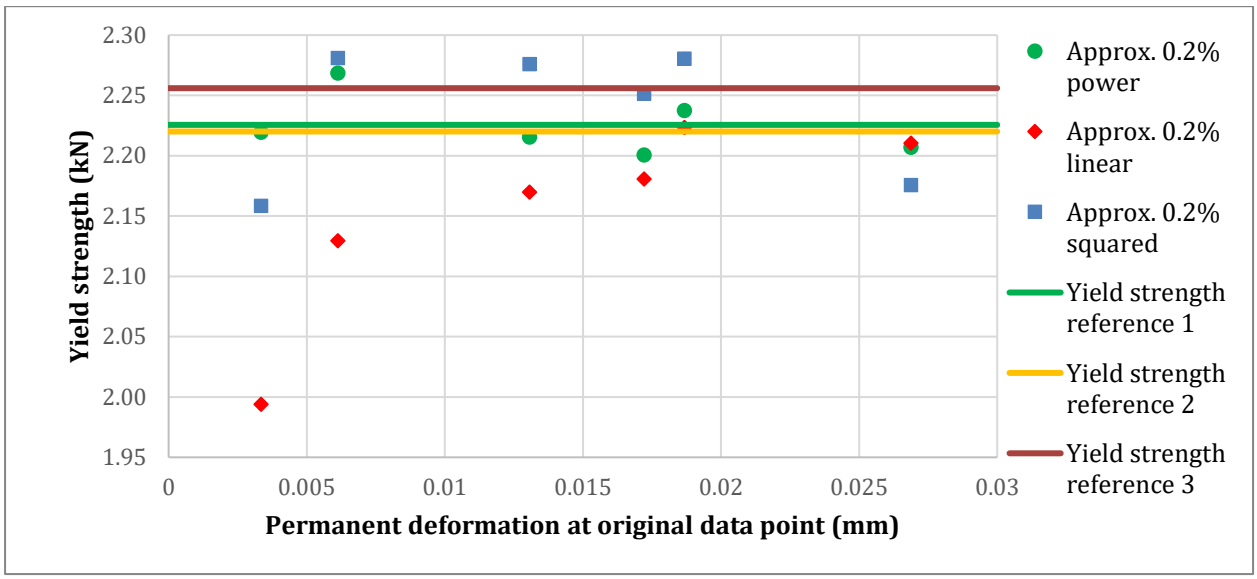

Figure 48: Approximated yield strength at 23°C compared to references.

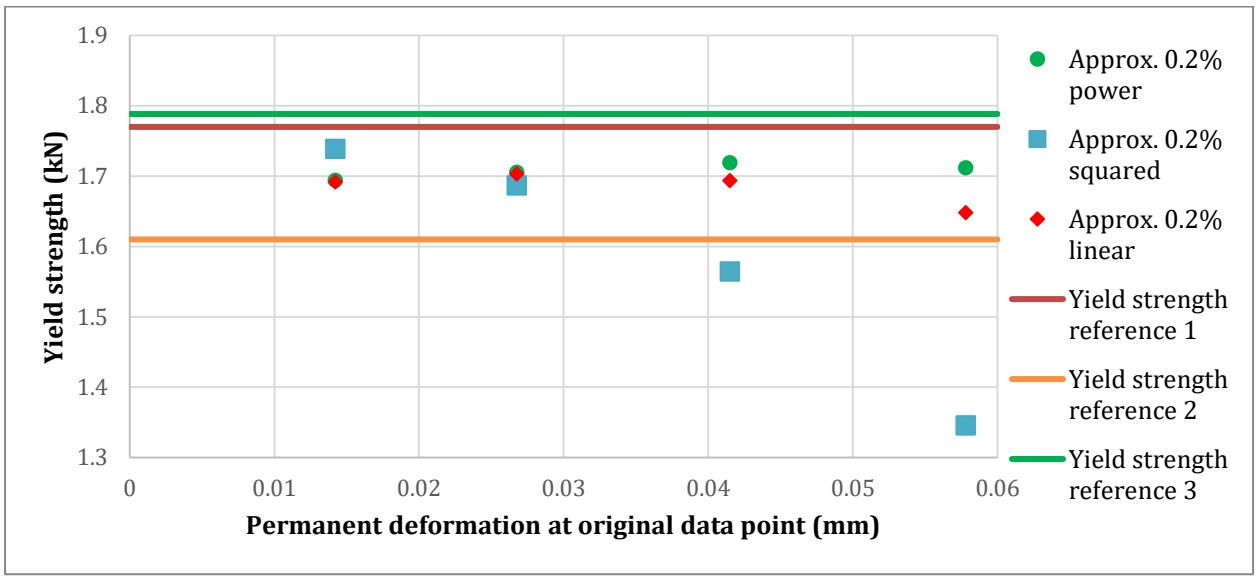

Figure 49: Approximated yield strength at 300°C compared to references.

Overall, the power function is consistently the most accurate way of approximating the yield strength. The linear and quadratic functions are the only approaches that have points that come nowhere close to approximating the real yield strength. These points are the ones below 0.01 mm for 23°C and one above 0.055 mm for 300°C. Looking further into these data points gives the following insight, which may explain their large deviation. These points lie outside the interval the functions in Figures 45-47 are based on.

The linear function keeps increasing or decreasing outside the interval it is based on and the quadratic function suddenly shifts from increasing to decreasing at high deformation. This does not reflect the actual behaviour of a tensile sample being stretched. The power function, on the other hand, increases quickly and levels off at higher deformations, which does accurately portray the behaviour of a tensile sample under tension. This is why the approximation using the power function stays accurate, even outside the interval it is based on.

4.4.4 Application: acquiring the temperature dependent yield strength

The final measurement can now be performed. In it, a single sample is heated to 300°C, stretched until a maximal load rate is reached and relaxed to 0.2 kN. Then, it is brought to 200°C and stretched in the same manner. This is also done for 100°C and 23°C. This gives four segments of load vs displacement curves that, when put together, result in Figure 50.

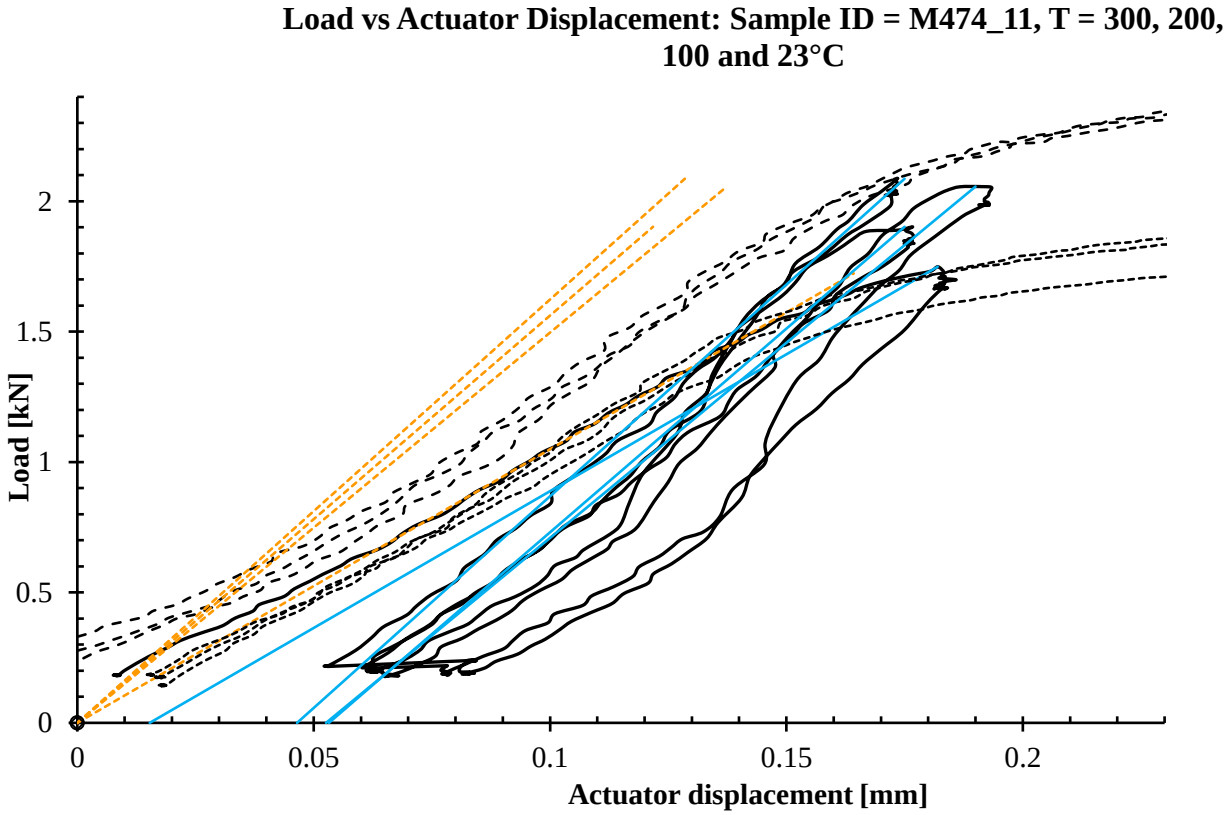

Figure 50: Interrupted tensile test at maximal load rate at 300, 200, 100 and 23°C on a single sample. The reference curves are added in dashed black lines. The orange dashed lines represent the slope of the elastic regions at different temperatures. The point where a blue line intersects with x-axis determines the permanent deformation at that temperature.

In a similar manner as before, the curves from Figures 45-47 are shifted to intersect with these points. The formulas of the curves for 100 and 200°C are derived from interpolation of the factors of the ones at 23 and 300°C. Then the value of these curves at 0.2% strain is calculated and displayed in Figure 51.

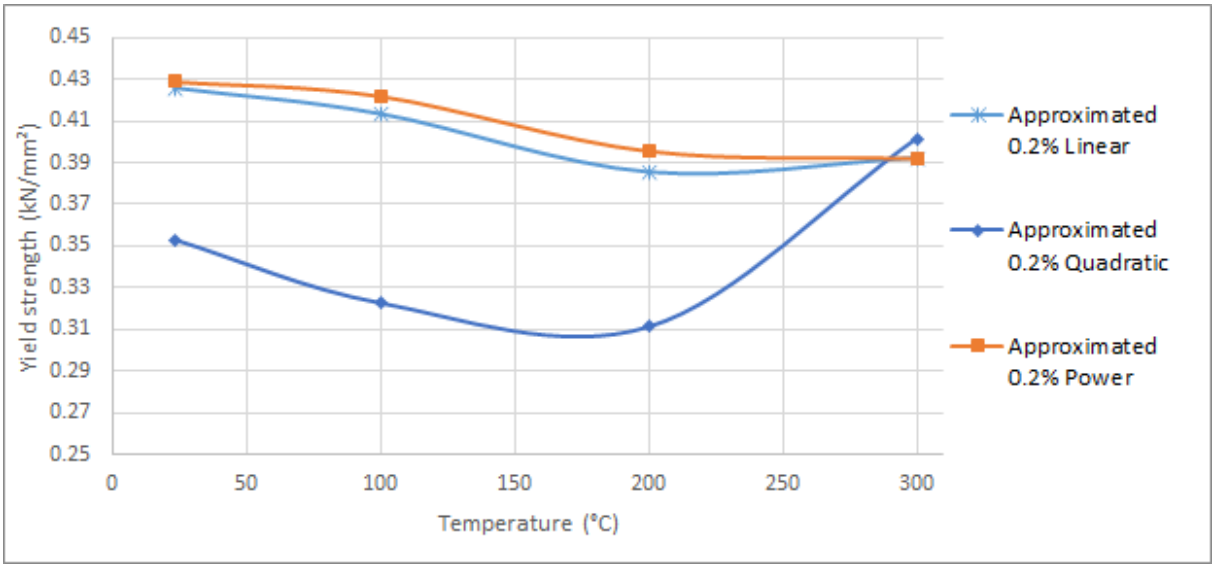

Figure 51: Extrapolated yield strengths for different temperatures through linear, quadratic and power function.

From measurements, it is known that the real yield strength vs temperature dependence is a monotonically decreasing function. By this criterium alone, the approximation using the power function is the only one that reflects reality. The final step is to compare these findings to some references. In Figure 52, the approximation of the yield strengths from the power function is compared to the references made earlier in this work and two more separate measurements of standard Eurofer97, one from 2006 (EU2T) and one from 2018 (c3,c9).

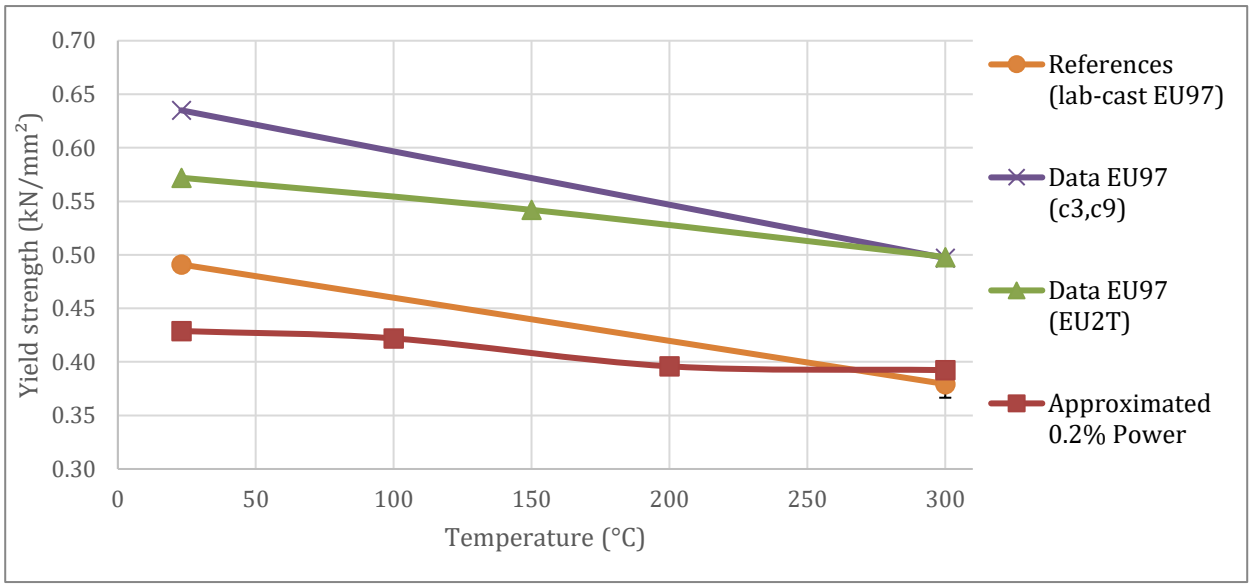

Figure 52: The approximated yield strengths at different temperatures compared to measurements of regular and lab-cast Eurofer. The error bars on the reference represent the standard error.

The absolute shift in yield strength between the approximation and the data of regular Eurofer97 can be attributed to the fact that regular Eurofer97 is being compared to lab-cast Eurofer. More importantly, however, is the slope of the graphs. If the absolute difference in yield strength is ignored at 300°C, the yield strength of the approximation at room temperature would undershoot the ones from the lab-cast references, the c3c9 samples and the EU2T samples by 75, 101 and 40 MPa respectively.

The approximation at 300°C is fairly accurate compared to the measurement data of lab-cast Eurofer but the error becomes far larger than acceptable for low temperatures. A possible explanation for this is as follows. Because the data points are selected based on nominal load rate, and this nominal load rate indicates the first signs of deformation, relatively small strains were expected. Despite this, after the sample was strained for the fourth time, a total strain of 0.39% had accumulated. The curve used for approximation at 23°C (Fig. 48) was based on a strain interval of [0.11% ; 0.42%], yet its accuracy was only verified for strains up to 0.22% since that was the highest strain achieved during the interrupted test at nominal load rate at 23°C. Extending the domain of Figure 48 by taking data points from the reference curves at 23°C around 0.39% strain, using the formula for approximation and verifying its accuracy gives the result in Figure 53.

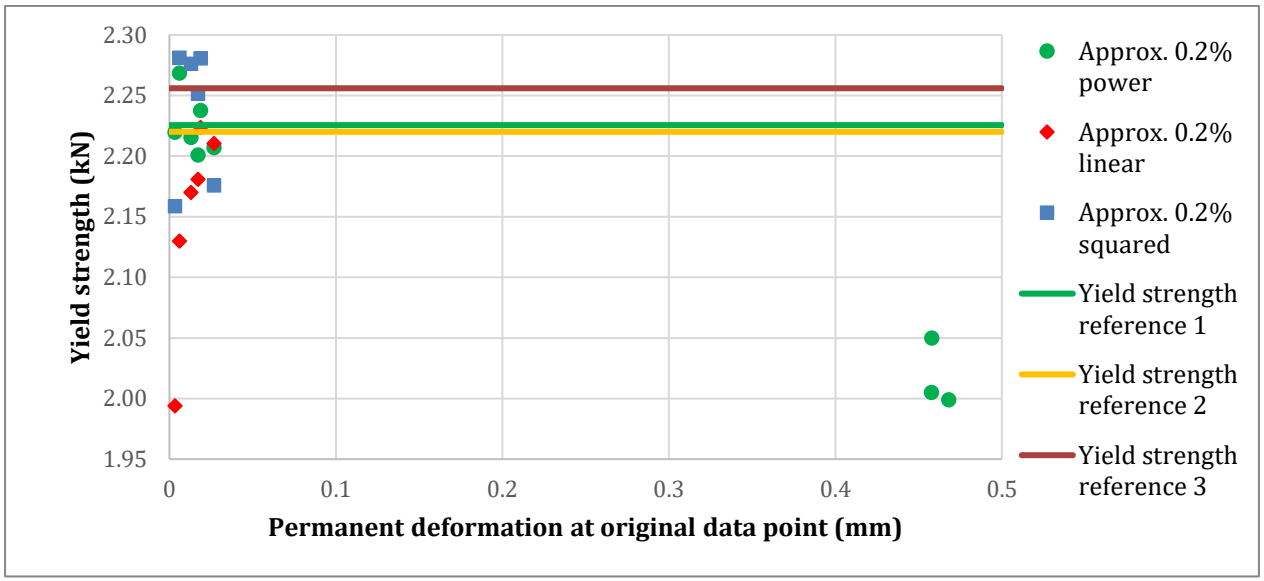

Figure 53: Approximated yield strength at 23°C compared to references with added data points at 0.39% strain.

These new data points give an approximation of the yield strength that is about 11% too low. This coincides with the yield strength at 23°C in Figure 52 undershooting the measured yield strength by 14%. Since the formulas for calculating the yield strength at 100 and 200°C are based on the formula for 23°C and the sample was already under high strain after the test at 200°C, this inaccuracy also partially affects the approximated yield strengths at 100 and 200°C.

5 CONCLUSIONS

This work started with the introduction to various analytical methods, namely the Vickers hardness test, the Charpy impact test and the tensile test. These techniques were taught and practiced such that, eventually they could be performed efficiently and without the need of supervision.
These tests were then used to analyse the flow properties of lab-cast Eurofer with dedicated heat treatment. From this, it was found that the DBTT of this lab-cast Eurofer was -125°C. Comparing this with the DBTT of standard Eurofer97, which is -80°C, it shows that the heat treatment significantly improved the low temperature flow properties of Eurofer.
Following that, a new procedure was tested. Its goal was to obtain the whole temperature dependent 0.2% yield strength from a single sample. To do this, certain steps had to be made first.
Reference curves were constructed at room temperature and 300°C so their 0.2% yield strength could be derived.
Interrupted tests based on fixed loads were performed at room temperature and 300°C. These curves were consistent with the references, showing the equivalence between both testing methods.
An interrupted test procedure based on load rate was practiced at room temperature and 300°C. Data points from these curves were used to predict the 0.2% yield strength and their results were found to be consistent with the established references.
The procedure was then applied to derive the 0.2% yield strength at 300, 200, 100 and 23°C from a single sample. The resulting temperature dependence was found to be fairly accurate for high temperature but suffers from an error that increases as the temperature decreases. This is likely due to the fact that by the time the test at room temperature was performed, the sample was heavily deformed, and the approximation at room temperature became less accurate as the strain increased.

REFERENCES

[1] "ITER - the way to new energy." [Online]. Available: https://www.iter.org/. [Accessed: 6-Jan-2019].

[2] "Fusion Energy for Our Future - Fusion 4 Freedom." [Online]. Available: https://fusion4freedom.com/. [Accessed: 7-Jan-2019].

[3] S. J. Zinkle and J. T. Busby, "Structural materials for fission & fusion energy," *Mater. Today*, vol. 12, no. 11, pp. 12–19, 2009.

[4] R. L. Klueh, "Elevated-Temperature Ferritic and Martensitic Steels and Their Application To Future Nuclear Reactors," Oak Ridge National Laboratory, Tennessee, 2004.

[5] M. J. Konstantinovic, "Advanced experiments to characterize radiation damage in nuclear materials" SCKCEN Mol – Belgium, 2019.

[6] S. J. Zinkle and N. M. Ghoniem, "Operating temperature windows for fusion reactor structural materials," *Fusion Eng. Des.*, vol. 51–52, no. 2000, pp. 55–71, 2000.

[7] R. Lindau *et al.*, "Present development status of EUROFER and ODS-EUROFER for application in blanket concepts," *Fusion Eng. Des.*, vol. 75–79, no. 0, pp. 989–996, 2005.

[8] J.-L. Boutard, A. Alamo, R. Lindau, and M. Rieth, "Fissile core and Tritium-Breeding Blanket: structural materials and their requirements," *Comptes Rendus Phys.*, vol. 9, no. 3–4, pp. 287–302, May 2008.

[9] K. C. Sahoo, J. Vanaja, P. Parameswaran, V. D. Vijayanand, and K. Laha, "Effect of thermal ageing on microstructure, tensile and impact properties of reduced activated ferritic-martensitic steel," *Mater. Sci. Eng. A*, vol. 686, no. October 2016, pp. 54–64, 2017.

[10] W. Wang, J. Chen, and G. Xu, "Effect of thermal aging on grain structural characteristic and Ductile-to-Brittle transition temperature of CLAM steel at 550 °C," *Fusion Eng. Des.*, vol. 115, pp. 74–79, 2017.

[11] R. Weyer, "The Modelling of Damage due to Diffusional Creep in High Chromium Steels," University of Cape Town, 2016.

[12] A. F. Tavassoli *et al.*, "Materials design data for reduced activation martensitic steel type EUROFER," *J. Nucl. Mater.*, vol. 329–333, P, no. 0, pp. 257–262, 2004.

[13] B. Bornschein, C. Day, D. Demange, and T. Pinna, "Tritium management and safety issues in ITER and DEMO breeding blankets," *Fusion Eng. Des.*, vol. 88, no. 6–8, pp. 466–471, 2013.

[14] S. D. Yadav, B. Sonderegger, M. Stracey, and C. Poletti, "Modelling the creep behaviour of tempered martensitic steel based on a hybrid approach," *Mater. Sci. Eng. A*, vol. 662, pp. 330–341, 2016.

[15] F. Abe, "Bainitic and martensitic creep-resistant steels," *Curr. Opin. Solid State Mater. Sci.*, vol. 8, no. 3–4, pp. 305–311, Aug. 2004.

[16] H. Aït Abderrahim, D. De Bruyn, G. Van den Eynde & S. Michiels (2013) Transmutation of High Level nuclear Waste by means of Accelerator Driven System (ADS).

[17] "IFMIF-DONES International Fusion Materials Irradiation facility – DEMO Oriented Neutron Source" [Online]. Available: http://www.roadmap2018.esfri.eu/projects-and-landmarks/browse-the-catalogue/ifmif-dones/. [Accessed: 2-Jun-2019].

[18] "EERA EUROPEAN ENERGY RESEARCH ALLIANCE Management Report" [Online]. Available: https://www.eera-set.eu/wp-content/uploads/JPNM_Management_Report_2016.pdf. [Accessed: 24-May-2019].

[19] Q. Huang, "Development status of CLAM steel for fusion applications," pp. 649, Sep. 2014.

[20] H. Li, D. Mitchell, "Microstructural characterization of P91 steel in the virgin, service exposed and post-service re-normalized conditions," 2013

[21] "P91 Material" [Online]. Available: https://www.multimetalsindia.com/blog/astm-a335-p91-material/ [Accessed: 21-Mar-2019].

[22] G. Mazzone, *et al.* "Choice of a low operating temperature for the DEMO EUROFER97 divertor cassette" *Fusion Engineering and Design,* vol. 124, pp 655-658, Nov 2017.

[23] E. Materna-Morris et al., "Structural material EUROFER97-2, Characterization of Rod and Plate Material: Structural, Tensile, Charpy and Creep Properties," Institut für aterialforschung, Forschungszentrum Karlsruhe, 2007.

[24] "Scanning electron microscopy" [Online]. Available: https://www.nanoscience.com/techniques/scanning-electron-microscopy/ [Accessed: 26-May-2019].

[25] "Vickers hardness test" [Online]. Available: https://en.wikipedia.org/wiki/Vickers_hardness_test. [Accessed: 15-Feb-2019].

[26] D. Tabor, "The Hardness of Metals," pp. 112.

[27] "Effect of Specimen Geometry on Tensile Testing Results" [Online]. Available: https://www.admet.com/effect-specimen-geometry-tensile-testing-results/. [Accessed : 29-May-2019]

[28] G. F. Pittinato, V. Kerlins, A. Phillips, M. A. Russo, "SEM/TEM FRACTOGRAPHY HANDBOOK" pp. 25-51, Dec 1975.

[29] A. Puype, "Investigation of Processing Routes, Microstructures and Mechanical Properties of Reduced Activation Ferritic/Martensitic Steels for Nuclear Fusion Applications," pp. 269-270, Sep 2018